

MASTER THESIS



# DESIGN OF A COMPLIANT MAGNETIC CAPSULE ROBOT FOR UNTETHERED CARDIOVASCULAR SURGICAL TOOLS

G.M. van Vliet

FACULTY OF ENGINEERING TECHNOLOGY  
DEPARTMENT OF BIOMECHANICAL ENGINEERING

## EXAMINATION COMMITTEE

Prof. Dr. Ir. S. Misra  
Dr. V. Kalpathy venkiteswaran  
Dr. Ir. R.G.K.M. Aarts

## DOCUMENT NUMBER

BE - 834

Thesis submitted by  
**G.M. van Vliet, BSc**  
under the supervision of  
**Prof. Dr. Ir. S. Misra,**  
**Dr. V. Kalpathy Venkiteswaran,** and  
**Dr. Ir. R.G.K.M. Aarts**  
in order to fulfill the necessary requirements to obtain a Master's degree in  
Biomechanical Engineering at the University of Twente  
and defended on  
**Tuesday, 9th of November, 2021**



## Acknowledgement

The report in front of you is the thesis for my graduation of the master Biomedical Engineering at the University of Twente. It is the result of approximately eleven months of work at the Surgical Robotics Laboratory (SRL). Through every joyful success moment and every tough struggling moment in these eleven months, I learned and grew a lot both in my personal and professional life. For all this I am very grateful.

I am grateful for all the opportunities and support I have been given by Prof. Dr. Sarthak Misra and Dr. Venkatsubramanian Kalpathy Venkiteswaran. This report would not have been possible without all facilities of the SRL. The daily supervision of Dr. Kalpathy Venkiteswaran guided me to this result. The conversations we have had helped me excessively to design and test the capsule robot. His overview and pressure-free guidance has brought back my overview and motivation several times. His suggestions and insights elevated the capsule robot and this thesis to the next level.

Besides this, I am generally thankful for the other SRL members. The readiness of everyone to help each other is extraordinary. In addition, I enjoyed the talks and fun we have had. I especially want to mention my gratitude to Mert Kaya, Michiel Richter, Onno Derkman, and Christoff Heunis for their help and their insights.

I am also grateful for my family and friends who supported me. Their presence in my life formed me to the person I am today. Without them and their support I would not have been able to complete my studies and this thesis.

Finally and above all, I am grateful for everything that God has done in me and my life. His faithfulness and love have brought me above everything else to this point. In uncertainty of the end point I may continue to walk every journey in life while often encountering my own weaknesses. In these weaknesses His strength becomes clear. Everything in this report is a testimony of the works of His hands. He guided me to this end point, which is the start of a new journey.

Chiel van Vliet  
November 9, 2021

## Abstract

Minimally invasive surgery has emerged over the last few decades as an important approach to treat many diseases. Research has developed and optimized many (robotic) medical systems to reduce invasiveness and increase the possibilities within this area. Remote structures in the human body could be reached in an even less invasive way by investigating new MIS methods. Untethered capsule robots are used for diagnosis in the digestive tract. However, these capsule robots are limited to diagnosis in the digestive tract. This study investigates a wireless approach to enable the development of untethered cardiovascular surgical tools. The prototype presented in this research is a compliant magnetic capsule robot (CMCR) which provides a base for milli-scale surgical tools in the abdominal aorta. The CMCR consists of a flexible inner core for flexibility in the axial direction, circular flexures for radial adaptability, permanent ring-magnets for actuation and flexible threads for tissue compliance and movement. The outer, default diameter of the capsule is 21 mm which fits in the abdominal aorta. Untethered actuation of the capsule robot is accomplished with an external magnetic field which interacts with the permanent ring-magnets of the robot. Experiments are performed on the capsule robot at three different scales ( $1.00\times$ ,  $1.25\times$  and  $1.50\times$ ) to demonstrate as a proof-of-concept for these type of untethered cardiovascular intervention tools. The results show the capsule robot moving through straight and curved acrylic tubes with different diameters. Besides this, experiments in a gelatin-coated tubes with an inner diameter (ID) of 26 mm show movement when the ( $1.25$ -scale) CMCR prototype is not compressed. However, the  $1.25$ -scale CMCR damaged the gelatin-coating in experiments with an ID21 mm gelatin-coated tube. Stagnation of the robot's movement is observed in a flexible tapered tube. The CMCR holds steady in a liquid flow and a minimally invasive insertion method with the CMCR embedded in ice is successfully tested. These results demonstrate desired and promising movement and adaptability of the capsule robot which provides a proof-of-concept for these type of robots. Nevertheless, some drawbacks show that many improvements need to be made before an application-ready, compliant, and stable base for untethered cardiovascular surgical intervention tools is reached.

## Samenvatting

Minimaal invasieve chirurgie is gedurende de laatste paar decennia ontwikkeld tot een belangrijke methode voor de behandeling van ziektes. Onderzoek heeft vele (robotische) systemen ontwikkeld en geoptimaliseerd om de invasiviteit te verminderen en de mogelijkheden op dit gebied te vergroten. Door onderzoek naar nieuwe MIS-methoden kunnen slecht bereikbare structuren in het menselijk lichaam op een minder invasieve manier worden bereikt. Draadloze capsulerobots worden al gebruikt voor diagnose in het spijsverteringskanaal. Deze capsulerobots zijn echter beperkt tot diagnose in het spijsverteringsstelsel. Deze studie onderzoekt een draadloze benadering om de ontwikkeling van ongebonden cardiovasculaire chirurgische instrumenten mogelijk te maken. Het prototype dat in dit onderzoek wordt gepresenteerd, is een adaptieve magnetische capsulerobot (CMCR) die een basis vormt voor chirurgische instrumenten op millischaal in de abdominale aorta. De CMCR bestaat uit een flexibele binnenkern voor flexibiliteit in axiale richting, cirkelvormige bladveren voor radiale aanpasbaarheid, permanente ringmagneten voor beweging, en flexibel schroefdraad voor weefselcompliance en beweging. De buitenste, standaarddiameter van de capsule is 21 mm, wat in de abdominale aorta past. Draadloze aansturing van de capsulerobot wordt bereikt met een extern magnetisch veld die een interactie aangaat met de permanente ringmagneten van de robot. Er zijn experimenten uitgevoerd op drie verschillende schalen van de capsulerobot ( $1.00\times$ ,  $1.25\times$  en  $1.50\times$ ) om proof-of-concept te demonstreren voor dit soort draadloze cardiovasculaire instrumenten. De resultaten tonen aan dat de capsulerobot door rechte en gebogen plexiglas-buizen met verschillende diameters beweegt. Daarnaast laten experimenten in gelatine-gecoate buizen met een binnendiameter van 26 mm beweging zien wanneer de CMCR-prototype ( $1.25$ -schaal) niet wordt samengedrukt. De CMCR met een schaal van  $1.25$  beschadigde echter de gelatine-coating in experimenten met een gelatine-gecoate buis van binnendiameter 21 mm. Stagnatie van de beweging van de robot wordt waargenomen in experimenten met een flexibele taps toelopende buis. De CMCR blijft stabiel in vloeistofstroom en een minimaal invasieve inbrengmethode met de CMCR ingebed in ijs is met succes getest. Deze resultaten demonstreren gewenste en veelbelovende beweging en aanpasbaarheid van de capsulerobot die een proof-of-concept biedt voor dit soort draadloze robots. Desalniettemin tonen enkele nadelen aan dat er veel verbeteringen moeten worden aangebracht voordat een toepassingsklare, aanpasbare en stabiele basis voor draadloze cardiovasculaire chirurgische instrumenten is bereikt.

# Table of Contents

|  |           |
|--|-----------|
| Acknowledgement                                | i         |
| Abstract                                       | ii        |
| Samenvatting                                   | iii       |
| Table of Contents                              | iv        |
| List of Figures                                | v         |
| List of Tables                                 | v         |
| <b>1 Introduction</b>                          | <b>1</b>  |
| 1.1 Thesis Outline . . . . .                   | 1         |
| <b>2 Preliminary Design</b>                    | <b>2</b>  |
| 2.1 Design Requirements . . . . .              | 2         |
| 2.2 Concepts . . . . .                         | 3         |
| <b>3 Compliant Magnetic Capsule Design</b>     | <b>3</b>  |
| 3.1 Radial Adaptability . . . . .              | 3         |
| 3.2 Axial Flexibility . . . . .                | 4         |
| 3.3 Magnetically-Actuated Movement . . . . .   | 5         |
| 3.4 Prototype fabrication & Scaling . . . . .  | 5         |
| <b>4 Modeling Flexure Stiffness</b>            | <b>6</b>  |
| <b>5 Prototype Experiments</b>                 | <b>8</b>  |
| 5.1 Motion Experiments . . . . .               | 8         |
| 5.2 Radial Adaptability Experiments . . . . .  | 8         |
| 5.3 BigMag System Motion Experiments . . . . . | 10        |
| 5.4 Additional Experiments . . . . .           | 10        |
| <b>6 Discussion</b>                            | <b>11</b> |
| <b>7 Conclusions &amp; Future Work</b>         | <b>12</b> |
| <b>References</b>                              | <b>13</b> |
| <b>A Design &amp; Design Process</b>           | <b>15</b> |
| A.1 Design Objective . . . . .                 | 15        |
| A.2 Objective Adjustment . . . . .             | 15        |
| A.3 Requirements & Constraints . . . . .       | 15        |
| A.4 Functional Design . . . . .                | 16        |
| A.5 Conceptual Design . . . . .                | 16        |
| A.6 Basic Experiments . . . . .                | 16        |
| A.6.1 Movement . . . . .                       | 17        |
| A.6.2 Passive Radial Flexibility . . . . .     | 18        |
| A.6.3 Passive Axial Flexibility . . . . .      | 18        |
| A.7 Full system concept . . . . .              | 19        |
| <b>B Hand sketches of full system concepts</b> | <b>21</b> |
| <b>C Robosoft Conference Paper</b>             | <b>24</b> |

## List of Figures

|     |   |    |
|-----|---|----|
| 1   | Functionality overview of the capsule robot. . . . .  | 1  |
| 2   | Design of the compliant magnetic capsule robot. . . . .   | 3  |
| 3   | Overview of different dimensions of the capsule robot and their symbols. . . . .                  | 4  |
| 4   | An overview of the magnetic working principle and a prototype of the capsule robot. . . . .       | 5  |
| 5   | Stiffness modeling of flexure pairs. . . . .  | 7  |
| 6   | Results of stiffness modeling of flexure pairs. . . . .   | 8  |
| 7   | Results of the motion experiments. . . . .  | 9  |
| 8   | Results of the radial adaptability experiments. . . . .   | 9  |
| 9   | Results of the experiments with the BigMag system. . . . .  | 10 |
| 10  | Results of the additional experiments. . . . .  | 11 |
| A.1 | A schematic cross-section overview of the device and its functions within a blood vessel. . . . . | 16 |
| A.2 | An example of a hand sketch of a full system concept. . . . .                                     | 17 |
| A.3 | Overview of manufacturing and assembling of movement prototypes. . . . .                          | 17 |
| A.4 | Overview of different versions of the passive radial flexibility concept. . . . .                 | 18 |
| A.5 | Overview of different concepts for axial flexibility. . . . .                                     | 19 |
| A.6 | Prototype of the capsule robot . . . . .  | 19 |
| A.7 | Hand sketch of full system concept 1. . . . .   | 21 |
| A.8 | Hand sketch of full system concept 2. . . . .   | 22 |
| A.9 | Hand sketch of full system concept 3. . . . .   | 23 |

## List of Tables

|   |   |    |
|---|---|----|
| 1 | The design requirements of the compliant magnetic capsule robot. . . . .  | 2  |
| 2 | Dimensions of the three different scaled prototypes of the compliant magnetically-actuated capsule robot. . . . . | 6  |
| 3 | Evaluation of the design requirements of the compliant magnetic capsule robot. . . . .                            | 12 |

# 1 Introduction

Minimally Invasive Surgery (MIS) has emerged over the last few decades as an indispensable approach in many surgical disciplines [1]. Advantages such as less postoperative pain and quick recovery make MIS more desirable than open surgery in many cases [2]. Regardless of these advantages, minimally invasive procedures also introduce more complexity for surgeons. Research into novel medical devices tries to overcome this complexity and to broaden minimally invasive diagnosis and therapeutic possibilities.

New (robotic) medical devices developed in research enable progress of MIS [3–5]. In the last decade the development of these systems evolved from large rigid platforms towards small, task-specific flexible systems. This improves accessibility of delicate and confined areas in the body which were previously difficult or impossible to reach [4–6].

Within surgical robotic devices, tethered continuum robots show some favorable MIS characteristics, such as their compliance and the ability to navigate narrow curved passages [5, 7–9]. These properties are utilized in MIS tools like magnetic sub-millimeter-diameter guidewires [10] and tendon-driven concentric tube robots [9]. Nevertheless, tethered flexible devices are limited in maneuverability and are not able to reach and perform surgical tasks in many minuscule areas within the body [11].

As an alternative to these wired systems, possibilities in mobile milli-/ microrobots are investigated to reach the remote body sites in even less invasive ways [6, 11]. Commercialized wireless capsule endoscopes (e.g. Medtronic’s Pillcam® and IntroMedic’s MiroCam®) emerged from such studies and have already been accepted as a standard in clinics for diagnosis of specific gastrointestinal diseases [12–14]. The clinical functionality of these capsule endoscopes has recently been expanded through the introduction of magnetically actuated capsule endoscopes (MACEs) in clinics [15] (AnX Robotica’s NaviCam®).

Although MACEs successfully achieve image-based gastrointestinal diagnosis, they are unable to perform biopsy or any other surgical intervention [14]. Magnetically-actuated soft capsule endoscopes (MASCEs) combine these untethered capsules with soft robotics to accomplish untethered surgical interventions. Research suggests surgical feasibility with these MASCEs [16, 17].

Capsule endoscopes, including MACEs and MASCEs mainly focus on the digestive tract [16, 18] where relatively more space is available compared to the cardiovascular system. Narrower tubular structures in the cardiovascular system might need a different approach which should take into account the effect of blood flow. Research suggests

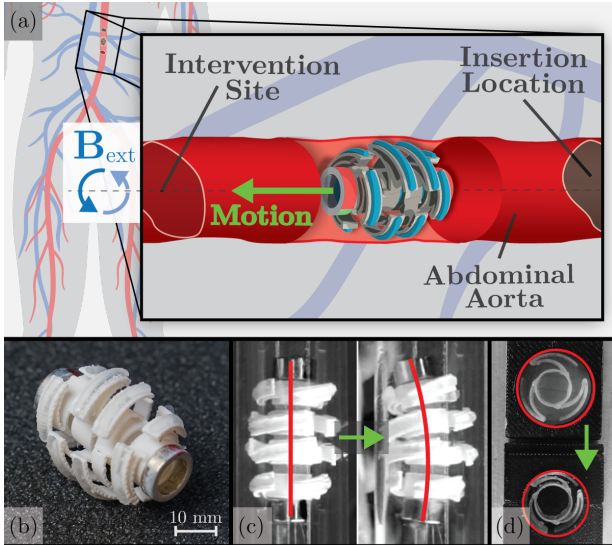


Figure 1: Overview of the Compliant Magnetic Capsule Robot (CMCR). (a) Conceptual sketch of CMCR moving between the insertion location and intervention site in the abdominal aorta under the influence of a rotational external magnetic field ( $B_{ext}$ ). (b) Prototype of the CMCR. (c) The CMCR has axial flexibility which allows it to bend along its long axis and move through curved vessels. (d) Radial compressibility of the CMCR ensures it maintains contact with the vessel wall when moving through sections of varying diameter.

that some possible approaches can be found in magnetic microrobots [19, 20] and soft robots [21]. Nevertheless, research into capsule millirobots which provide a stable base for interventions in narrow tubular structures of the cardiovascular system is lacking. Such a base can passively anchor to the blood vessel at a target location, withstanding blood flow to enable stability for surgical interventions in the dynamic environment of cardiovascular system.

This study explores the feasibility of using untethered capsule robots for interventions in the cardiovascular system. The design, optimization, and testing of an untethered compliant magnetically-actuated capsule robot (CMCR) for the abdominal aorta (Fig. 1) is presented to demonstrate a proof-of-concept of these type of robots. The focus of the CMCR is to combine the compliance of soft robots, the continuous flexibility of continuum robots, the convenience of capsule endoscopes, and magnetic actuation. This focus is embraced to obtain a capsule robot which serves as a harmless, mobile and stable anchor for cardiovascular surgical interventions such as stent placement.

## 1.1 Thesis Outline

This study starts by setting the outlines of the design with the preliminary design in Section 2. Section 3 elaborates the design, and Section 4 derives

Table 1: The design requirements of the compliant magnetic capsule robot.

| Requirements | Description  |   |
|--------------|--|---|
| R1           | Default outer diameter of the CMCR ( $d_0^r$ ) should be slightly larger than the average aortic diameter ( $d_a$ )  | $d_0^r <^\epsilon d_a \rightarrow d_{r,0} \approx 21$ mm [22, 23] |
| R2           | Diameter of the capsule robot ( $d_r$ ) should adapt to aortic diameter fluctuations ( $\delta_a$ )  | $d_r = d_0^r - \delta_a$ where $\delta_a > 2.3$ mm                |
| R3           | Movement of the capsule robot should be controlled wirelessly by an external magnetic field  | Magnetically-actuated movement                                    |
| R4           | Capsule robot should move through 50° curves ( $\alpha_c$ ) with an 70 mm arch length ( $L_c$ ) in the abdominal aorta                                     | $\alpha_c = 50^\circ$ with $L_c = 70$ mm                          |
| R5           | The CMCR should not damage the blood and aortic wall: biocompatible & elastic modulus CMCR ( $E_r$ ) equal to elastic modulus artery ( $E_a$ )             | Biocompatible,<br>$E_r \approx E_a \in [0.1, 1]$ MPa              |
| R6           | Cross-sectional area of the robot ( $A_r$ ) should permit acceptable blood flow through the (assumed circular) cross-sectional area of the aorta ( $A_a$ ) | $A_r < 0.7A_a$  |
| R7           | The robot should function within the aortic blood flow ( $Q_a$ )   | $Q_a = 2.9 \pm 0.6$ L/min   |

a mathematical model for optimization of the design. Section 5 explains the experiments and presents the experimental results. Section 6 discusses the results and conclusions are drawn in Section 7.

## 2 Preliminary Design

The preliminary design of the capsule robot is discussed in this section. Several design requirements are formulated to set the boundaries for the design (Table 1). With these requirements in mind, several concepts for the CMCR are drafted before moving toward a final design.

### 2.1 Design Requirements

Design requirements for the CMCR are drafted with medical and physical limitations in mind to set the boundaries for the capsule robot design. Table 1 summarizes these requirements.

*Capsule diameter (R1)* - The first limitation for the capsule robot is the available space within the aimed cardiovascular structure. The abdominal aorta was chosen for proof-of-concept demonstration given its relatively large average diameter. Research reports normal average abdominal aortic diameters ranging between 12 mm and 27 mm [22, 23]. The mean of this range is approximately 20 mm. The default diameter of the CMCR should be slightly larger than the average abdominal aortic diameter to make it clinically relevant and to provide some stability with the compressive forces due to the radial elasticity of the artery. Therefore, the CMCR’s default diameter should be approximately 21 mm.

*Radial Adaptability (R2)* - The diameter of the abdominal aorta fluctuates — just like many blood vessels — in the different segments of the artery. Contact between the robot and the artery wall is required to maintain stability. For this reason, the capsule robot should have the ability to adapt its diameter to the varying artery diameter. The minimal relevant diameter reduction for the robot is 2.3 mm considering the range of diameters in different segments of the abdominal aorta [22]. Passive components like spring elements could adapt the CMCR without external actuation. Passivity is desirable for this radial adaptability to keep active actuation options for others functions such as movement. Besides, active actuation of this radial adaptability would require challenging untethered control given the necessity for constant adaptation.

*Magnetically-Actuated Movement (R3)* - The CMCR should move wirelessly within the abdominal aorta. Research shows that magnetic actuation is very suitable for this in vivo wireless actuation [24] given its human-safe operation, wireless actuation and rapid response. This magnetic actuation approach for the movement of the robot is chosen given this suitability, and the magnetic focus and possibilities of the Surgical Robotics Lab (SRL).

*Axial Flexibility (R4)* - Even though the abdominal aorta is relatively straight, curves are generally found in blood vessels. The CMCR should be able to move through curved blood vessels when considering the possible future extension of the CMCR’s application to other blood vessels. The maximum curve in the aorta is the aortic arc with an average arc angle of

107° over an arch length of approximate 71 mm [25]. Although this segment of the aorta is not located in the abdominal aorta, it provides a good reference for a maximum curve. Therefore, it is assumed that the CMCR should be able to move through curves with a curvature which is approximately 50% of this maximum curve. This means that the CMCR is required to move through a maximum curve of 50° over an 70 mm arch length.

*Biocompatibility and compliance (R5)* - Damaging blood cells or the abdominal aorta could cause severe problems for the human body. Therefore, the CMCR should be biocompatible and should execute all previously mentioned functions without harming the integrity of the abdominal aorta. To achieve this, the robot requires parts which are biocompatible and compliant to the aortic wall. Biocompatibility is attained by selecting biocompatible materials and compliance is achieved by smooth and soft materials with an elastic modulus approximately equal to that of the aortic wall. The elastic modulus of an artery is ranging approximately between 0.1 MPa and 1.0 MPa [26].

*Cross-sectional Area (R6)* - Besides damage to the cardiovascular system, the robot could cause damage to other tissues as well when obstructing the blood circulation. High risks for cardiovascular events occur in patients with high-grade vascular stenosis. High-grade stenosis indicates a vessel obstruction of  $\geq 70\%$  [27]. The cross-sectional area of the CMCR should block less than this 70% of the blood vessel to prevent high risks of tissue damage.

*Performance in Blood Flow (R7)* - Finally, the robot should perform properly within the blood flow through the abdominal aorta. At rest the average

blood flow in this artery is  $2.9 \pm 0.6$  L/min [28]. The CMCR should withstand the forces of this flow and operate in it.

## 2.2 Concepts

Several preliminary concepts for the CMCR have been drafted. The feasibility of each concept was considered with the requirements (Tab. 1) in mind. The two most promising concepts were selected, and some basic experiments were executed. The best performing concept in these tests is identified and is used in the rest of the design process. This complete process from preliminary design to best performing concept is elaborated in Appendix A. Some hand sketches of preliminary full system concepts can be found in Appendix B.

## 3 Compliant Magnetic Capsule Design

Various attributes for the design of the CMCR emerge in the design process from the design requirements. These attributes are passive radial adaptability, axial flexibility, and magnetic actuated movement. The elaboration of these attributes, and the merging of these into the design of the capsule robot is described in this section. An overview of this design and its dimensions can be found in Fig. 2 and Fig 3 respectively. The dimensions for the prototypes are summarized in Table 2.

### 3.1 Radial Adaptability

The CMCR requires a radial adaptable structure to adjust to the fluctuating aortic diameter in the

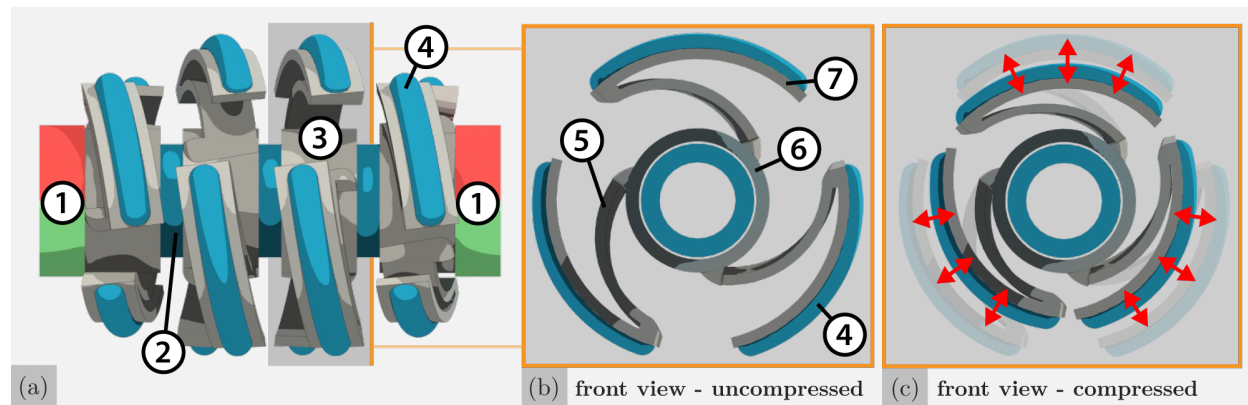


Figure 2: The design of the compliant magnetic capsule robot (CMCR). (a) Side view of the CMCR containing: ① permanent magnets, ② a flexible core, and ③ segments of flexure pairs. (b) Front view of a segment of flexure pairs consist of ④ a flexible thread (attached to the outer flexure to ensure soft contact with the vessel wall), ⑤ an inner flexure, and ⑦ an outer flexure in series. The inner part of the segment is a rigid core ⑥. (c) Front view of the CMCR showing compression of the flexure pairs and passive elastic restoration to the default diameter.

radial direction. An inner and outer structure are implemented in the robot to enable this adaptability. The outer structure (Fig. 2 - ⑦) can adapt to the environment, whereas the inner structure provides a stable core for the robot (Fig. 2 - ⑥).

Connecting elements are required between the inner and outer structure to keep the outer structure in place. Elasticity in these elements contributes to the adaptability of the outer structure during radial compression and the passive recoverability of the default diameter after compression. Spring elements are suitable for this application.

Blade flexures (Fig. 2 - ⑤) are selected for these connecting spring elements due to their scalability. Besides this, the fabrication of these blade flexures is simple, and the stiffness of these flexures can be easily tuned by changing the flexure properties such as flexure material, flexure length, and flexure thickness. The selected material for the flexures is ABS due to its elasticity properties at small scales. Despite these properties, the stiffness of ABS flexures is found to be relatively high for the radial adaptability of the milliscale CMCR. Nevertheless, the compression range of 5 mm is achieved by using a single blade flexure with a small as possible flexure thickness and a large as possible flexure length. The flexure radius is selected to be 6.65 mm and the flexure arc to be approximately 90°. A flexure length ( $L_{f,lr}$ ) of approximately 10 mm is the result of this.

Three 90° blade flexures are also used for the outer structure to allow shape adjustment. This means that the shape of the outer structure remains circular instead of triangular when radially compressed. Three 30° spaces between the flexures of the outer structure enable the radial compression of the CMCR. The default diameter of the outer structure ( $d_{lr,u}$ ) is set to 20 mm, and the diameter at full radial

compression ( $d_{lr,c}$ ) is estimated to be approximately 15 mm. By connection of these flexures (Fig. 2 - ⑦) to the connecting flexures (Fig. 2 - ⑤) in series flexure-pairs is formed. These flexure-pairs are attached to the core/ inner structure.

The core with the three flexure-pairs is 3D printed with ABSplus P430 (ABSplus P430, Stratasys, Ltd., Eden Prairie, MN, USA) on the Fortus 250mc FDM printer (Stratasys, Ltd., Eden Prairie, MN, USA). The flexure thickness of both flexures ( $t_f$ ) is set to the best resolution of this printer which is 0.7 mm.

### 3.2 Axial Flexibility

Flexibility in the axial direction of the CMCR is necessary for moving through the curves in the abdominal aorta. A flexible core (Fig. 2 - ②) is added to the capsule robot to achieve this axial flexibility. This flexibility is accomplished by 3D printing the core with Elastic 50A Resin (Formlabs, Somerville, MA, USA) on a Form 2 stereolithography (SLA) printer (Formlabs, Somerville, MA, USA). An axial channel is embedded in this cylindrical core (visible on the front view of Fig. 2) to allow blood flow through the capsule robot. The outer diameter of the core ( $d_{co}$ ) is 7.5 mm and the inner diameter ( $d_{ci}$ ) is 5 mm.

Axial bending of the radial adaptable structure (Fig. 2 - ③) is enabled by segmenting it into four segments with each three flexure-pairs. Two sizes of these flexure-pair segments are designed to give the CMCR a pill-like shape for a more gradual radial adaption. The large flexure-pairs segments have the previously mentioned dimensions (Sec. 3.1). The other, smaller flexure-pairs segments have a default diameter ( $d_{sr,u}$ ) of 16 mm and an estimated fully compressed diameter ( $d_{sr,c}$ ) of 12 mm. The flexure

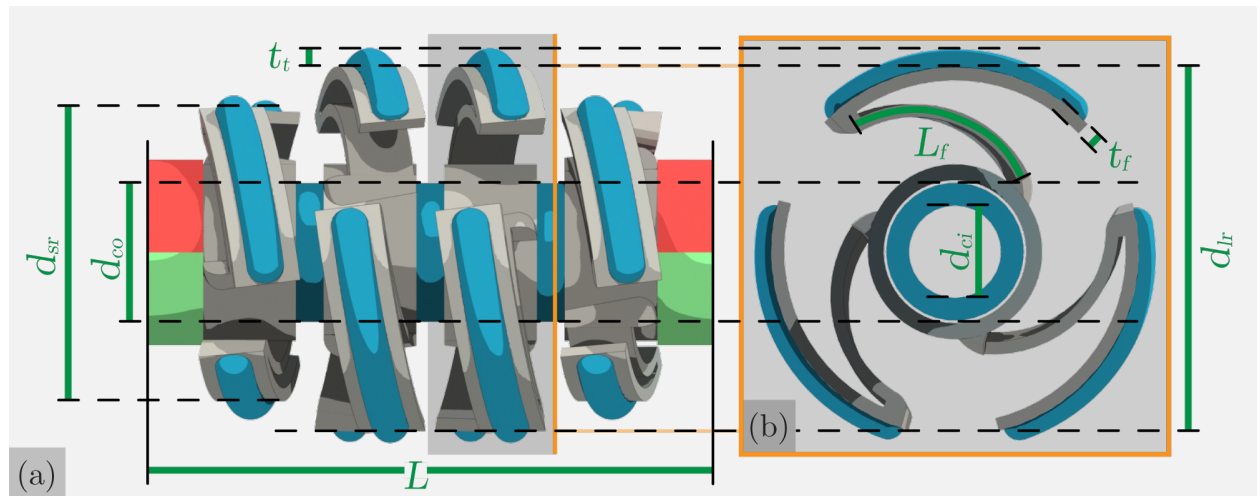


Figure 3: Overview of different dimensions of the compliant magnetic capsule robot (CMCR): Total capsule length ( $L$ ), flexible thread thickness ( $t_t$ ), flexure thickness ( $t_f$ ), flexure length ( $L_f$ ), large ring OD ( $d_{lr}$ ), small ring OD ( $d_{sr}$ ), flexible core OD ( $d_{co}$ ), and flexible core ID ( $d_{ci}$ ). (a) Side view of the CMCR. (b) Front view of the segment of flexure-pairs.

length of the connecting blade flexure in the small flexure-pair ring ( $L_{f,sr}$ ) is reduced to approximately 5.5 mm.

The rigid core of the flexure-pairs segments is connected to the flexible core by glueing with LOCTITE® 401 (Loctite, Hartford, CT, USA). Two of the large flexure-pairs segments are placed in the center of the flexible core and two small flexure-pairs segments are placed behind and before these large diameter segments. Space between the flexure-pairs segments is added to allow the slight rotation of the rigid segments when the flexible core is bent.

### 3.3 Magnetically-Actuated Movement

The CMCR should move steadily through the abdominal aorta by untethered magnetic actuation. Complicated actuation mechanisms are not suitable for the capsule robot given its dimensions. Sliding- or rotation-based methods offer simple and scalable mechanisms for movement. Rotation-based screw-like motion of helical-shaped magnetic robots has been demonstrated several times in research at micro- and milliscale [20, 29, 30]. Both backward and forward motion can be achieved with this helical robot shape by rotating the robot one way or the other with an external magnetic field. This screw-like motion is adopted in the CMCR given its simplicity and scalability.

The CMCR is embedded with permanent magnets (Fig. 2 - ①) to create an internal magnetic dipole along a radial direction. This internal magnetic dipole ( $\mu_{int}$ ) aligns with the external magnetic field ( $\mathbf{B}_{ext}$ ) when such a field is applied to the robot (Fig. 4a). A torque on the internal magnetic dipole is induced due to this alignment when the external field is rotated around the longitudinal axis of the

robot. This torque on the embedded dipole results in rotation of the capsule robot ( $V_{rot}$ ).

Rotational motion is generally transferred to longitudinal motion by using threads. The threads make contact with the environment which results due to the helical shape of the screw threads in a longitudinal force. Threads are applied to the outside of the CMCR to transfer the rotational motion of the robot into a longitudinal force which leads to longitudinal movement of the robot ( $V_l$ ). The direction of the longitudinal movement is turned by changing the direction of the rotational motion.

The internal dipole is created with two radially-magnetized permanent magnets which are glued on the ends of the flexible core of the CMCR with LOCTITE® 401. Two 10/7x3 mm ring magnets with a radial N45 magnetisation (Model R-10-07-03-DN, Supermagnete, Gottmadingen, Germany) have been selected for this internal dipole.

The threads are placed on the outside of the robot on the flexure-pairs (Fig. 2 - ④) and have a 10° pitch angle. Flexible material is used for these threads to improve the robot's compliance to the tissue of the aortic wall. These flexible threads are 3D printed with Elastic 50A Resin (Formlabs, Somerville, MA, USA) on a Form 2 stereolithography (SLA) printer (Formlabs, Somerville, MA, USA) and have a thickness ( $t_t$ ) of 1 mm. The threads are glued to the flexure-pairs with LOCTITE® 401 which gives the capsule robot an outer diameter of 21 mm.

### 3.4 Prototype fabrication & Scaling

Several flexure-pair properties such as thickness, material and configuration within the in-house possibilities are evaluated and tested to obtain optimal stiffness. Since no optimal stiffness was found, three different scales of the prototype are fabricated to test the performance with respect to

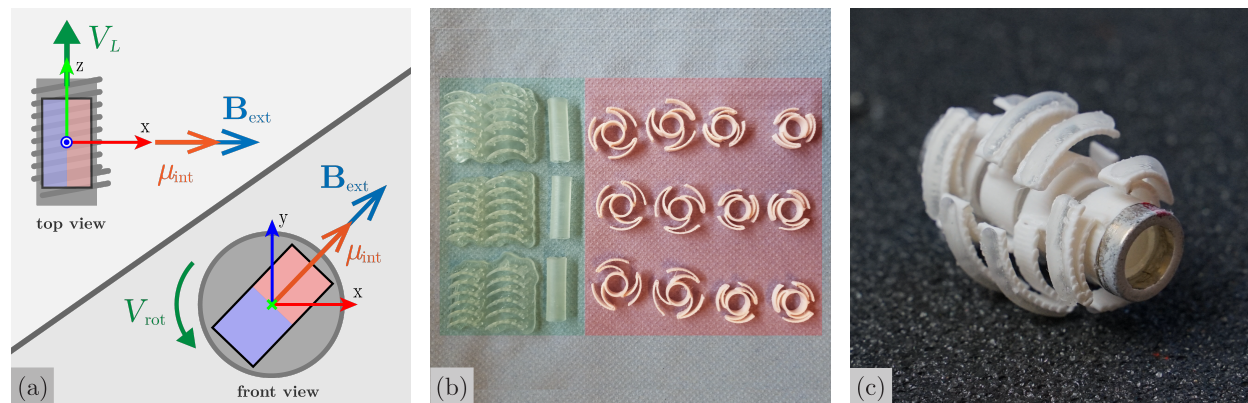


Figure 4: An overview of the magnetic principle and a prototype of the compliant magnetic capsule robot (CMCR). (a) Magnetic working principle for the CMCR: The internal magnetic dipole of the robot ( $\mu_{int}$ ) aligns with the external magnetic field ( $\mathbf{B}_{ext}$ ). Forward (or backward) motion ( $V_L$ ) is caused by screw-like rotational motion ( $V_{rot}$ ) due to the revolving of the external field. (b) 3D printed elastic (green) and solid ABS (red) parts for three prototype of the robot: threads (left), flexible core (mid) and the flexure-pairs segments (right). (c) Assembled prototype of the CMCR.

Table 2: Dimensions of the three different scaled prototypes of the compliant magnetically-actuated capsule robot (CMCR).

| Dimension                       | Symbol     | Prototype scale                  |                               |                               |
|---------------------------------|------------|----------------------------------|-------------------------------|-------------------------------|
|                                 |            | 1.00                             | 1.25                          | 1.50                          |
| Uncompressed OD (mm)            |            |                                  |                               |                               |
| - Large ring                    | $d_{lr,u}$ | 20.0                             | 24.8                          | 30.4                          |
| - Small ring                    | $d_{sr,u}$ | 16.0                             | 19.8                          | 24.3                          |
| Est. min. compressed OD (mm)    |            |                                  |                               |                               |
| - Large ring                    | $d_{lr,c}$ | 15                               | 18.6                          | 22.8                          |
| - Small ring                    | $d_{sr,c}$ | 12                               | 14.9                          | 18.3                          |
| Approx. flexure length (mm)     |            |                                  |                               |                               |
| - Large ring                    | $L_{f,lr}$ | 10                               | 12.5                          | 15                            |
| - Small ring                    | $L_{f,sr}$ | 5.5                              | 6.9                           | 8.3                           |
| Flexure thickness (mm)          | $t_f$      | 0.7                              | 0.7                           | 0.7                           |
| Flexible core OD (mm)           | $d_{co}$   | 7.5                              | 9.3                           | 11.4                          |
| Flexible core ID (mm)           | $d_{ci}$   | 5.0                              | 6.2                           | 7.6                           |
| Flexible threads thickness (mm) | $t_t$      | 1.0                              | 1.2                           | 1.5                           |
| Total capsule length (mm)       | $L$        | 30.5                             | 37.7                          | 49.2                          |
| Magnets (mm)                    |            | Ring: $\emptyset : 10, 7, h : 3$ | Disc: $\emptyset : 12, h : 6$ | Disc: $\emptyset : 12, h : 6$ |

stiffness of the circular flexures. The thickness of the flexures ( $t_f$ ) is kept equal to 0.7 mm to obtain a relatively lower stiffness since the thickness influences the second moment of area to the third power. The three scales (1.00 $\times$ , 1.25 $\times$  and 1.50 $\times$ ) are selected due to fabrication constraints.

The dimensions mentioned in Sec. 3.1, Sec. 3.2, and Sec. 3.3 describe the dimensions of the 1.00-scale prototype. The matching dimensions of the prototypes of the other scales can be found in Table 2. Two 12x6 mm disc magnets with a radial N42 magnetisation (Model S-12-06-DN, Supermagnete, Gottmadingen, Germany) are selected for the 1.25- and 1.50-scale prototypes.

The parts for the prototype are 3D printed with the previously specified dimensions and printers. An overview of these parts can be found in Fig. 4b. The parts and the permanent magnets are assembled to the capsule robot as seen in Fig. 4c.

## 4 Modeling Flexure Stiffness

The radial stiffness of the CMCR determines its adaptability to changing vessel diameters and the actuation field necessary to generate motion. In this section, a mathematical model is derived to calculate the stiffness of the flexure pairs on the CMCR.

A single flexure-pair of the capsule robot is modeled as two circular cantilever beams connected in series (Fig. 5a). The outer beam is in contact with the vessel wall, and therefore it is assumed that a distributed force ( $\bar{F}$ ) acts per unit length on the

outer beam. The inner beam is fixed at the root and the reaction loads from the outer beam act at the tip of the inner beam. For simplicity, only planar deflections (in the xy-plane as indicated in Fig. 5) are considered.

For a single beam, the deflection can be characterized using beam theory assuming bending-dominant behavior. Each beam is defined by its radius  $R$  and arc angle  $\psi$ , with arc length  $L = \psi R$ . The independent centerline coordinate  $s \in [0, L]$  and the coordinate-dependent slope  $\theta(s)$  are used to calculate the deflected shape using beam theory as

$$\theta'(s) = \frac{M(s)}{EI} + \frac{1}{R}, \quad (1)$$

with bending moment  $M(s)$ , second moment of area  $I$  and elastic modulus  $E$ . For a rectangular cross-section,  $I = wt^3/12$  with width  $w$  and thickness  $t$ .

For the analysis here, each beam is considered independently, with the deflection and reaction loads on the outer beam calculated first, followed by the inner beam. Following the methodology described by Venkiteswaran and Su [31], Eqn. (1) is differentiated with respect to the variable  $s$  and combined with two boundary conditions to obtain a set of equations that define beam behavior.

For the outer beam (Fig. 5b), the derivative of the bending moment in the z-direction is calculated as

$$dM_1^z(s) = \|\mathbf{s}^* \times d\mathbf{F}\|, \quad (2)$$

where

$$d\mathbf{F} = \bar{F} \cdot \begin{bmatrix} -\sin(\theta_1(s)) \\ \cos(\theta_1(s)) \end{bmatrix}, \quad (3)$$

and

$$\mathbf{s}^* = \begin{bmatrix} \int_s^L \cos \theta_1(s) ds \\ \int_s^L \sin \theta_1(s) ds \end{bmatrix}. \quad (4)$$

For planar deflections in the  $xy$ -plane, only the  $z$ -component of the bending moment acts on the beam. Therefore,

$$\theta_1''(s) = \frac{-dM_1^z(s)}{EI}. \quad (5)$$

For the outer beam, the slope at the fixed end ( $s = 0$ ) is zero. At the end of the beam ( $s = L$ ), the moment  $M_1^z(L_1)$  is zero. Therefore, the boundary conditions are

$$\theta_1(0) = 0, \quad \theta_1'(L_1) = \frac{1}{R_1}. \quad (6)$$

For the inner beam, the reaction force  $\mathbf{F}_P$  and reaction moment  $M_P^z$  at the connection point  $P$  (Fig. 5c) between the two beams must be calculated first. This force and moment are defined as

$$\mathbf{F}_P = \int_0^{L_1} d\mathbf{F} ds = \bar{F} \cdot \int_0^L \begin{bmatrix} -\sin(\theta_1(s)) \\ \cos(\theta_1(s)) \end{bmatrix} ds, \quad (7)$$

and

$$M_P^z = M_1^z(0). \quad (8)$$

Thus, for the inner beam,

$$\begin{aligned} \theta_2''(s) &= \frac{-dM_2^z(s)}{EI} \\ &= \frac{1}{EI} (F_P^x \sin \theta_2(s) - F_P^y \cos \theta_2(s)). \end{aligned} \quad (9)$$

The slope at the fixed end of the beam ( $s = 0$ ) is zero. The moment  $M_P$  acts at the other end of the beam ( $s = L$ ). This results in the boundary conditions

$$\theta_2(0) = 0, \quad \theta_2'(L_2) = \frac{M_P^z}{EI} + \frac{1}{R_2}. \quad (10)$$

Eqns. (5),(6),(9) and (10) form a set of differential equations and boundary conditions can be solved using numerical methods. The shape of the deflected beams can be calculated from the  $x$  and  $y$  coordinates as

$$x(s) = \int_s^L \cos \theta(s) ds \quad (11)$$

$$y(s) = \int_s^L \sin \theta(s) ds. \quad (12)$$

With these deflected beam shapes the mean change in radius ( $\delta_R$ ) of the flexure-pair is calculated across 10 points along the length of the outer beam. For a given input force  $F = L_1 \bar{F}$ , the stiffness of the flexure-pair  $k_{fp}$  is defined as

$$k_{fp} = F/\delta_R. \quad (13)$$

The reaction force from compression of the flexure pairs leads to friction between the CMCR and vessel wall. If  $N$  flexure pairs under radial compression  $\delta_R$

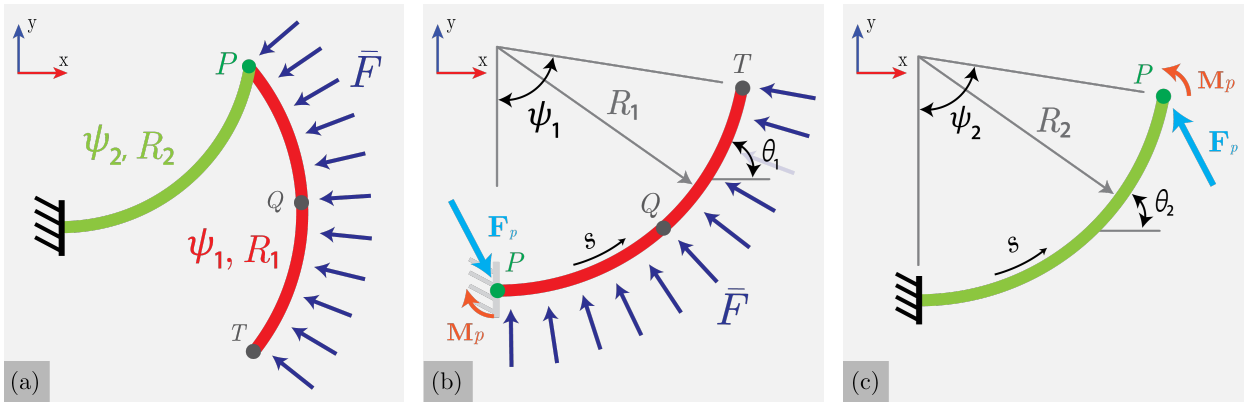


Figure 5: Stiffness modeling of flexure pairs. (a) The outer flexure experiences a distributed force per unit length ( $\bar{F}$ ), has undeflected radius ( $R_1$ ) and subtends an arc angle ( $\psi_1$ ). The inner flexure is fixed at the root, has undeflected radius ( $R_2$ ) and subtends an arc angle ( $\psi_2$ ). (b) The deflection of each beam is calculated using beam theory, with  $s$  representing the independent coordinate along the beam length, and  $\theta(s)$  the deflected orientation of the beam at  $s$ . Distributed load ( $\bar{F}$ ) on the outer beam (red) results in beam deformation and in a reaction force ( $\mathbf{F}_P$ ) and reaction moment ( $M_P$ ) in connection point  $P$ . (c) The reaction force and moment in point  $P$  results in deformation of the inner beam (light green).

are in contact with the vessel wall, the stall torque is given by

$$T_f = \mu_f N k_{fp} \delta_R (R - \delta_R), \quad (14)$$

where  $\mu_f$  is the coefficient of static friction between the CMCR and vessel wall. The CMCR is able to overcome the friction stall torque and move under an external magnetic field  $\mathbf{B}_{\text{ext}}$  if

$$T_f < T_B = \|\mu_{\text{int}} \times \mathbf{B}_{\text{ext}}\|, \quad (15)$$

where  $\mu_{\text{int}}$  is the total magnetic dipole moment of the CMCR and  $T_B$  is the induced magnetic torque.

The above condition can be used to determine the magnetic field necessary to move the CMCR. As an example, this is evaluated for one of the prototypes (1.50-scale) and tested under a uniform magnetic field (Sec. 5). The parameters for the analysis are given in Table ???. The coefficient of friction is assumed to be 0.8 for contact between the flexible thread made of rubber and the acrylic wall of the tubes used for experiments. The deflection of the flexure-pair is obtained for a range of  $\bar{F} \in [0, 200]$  N/m (Fig. 6a). It is noticeable that most of the deformation is concentrated on the outer flexure. The stiffness of the flexure-pairs decreases under deformation, as can be seen in Fig. 6b. The comparison between maximum magnetic torque and friction stall torque is given in Fig. 6c. For the 1.50-scale prototype, a magnetic field of 100 mT can move the CMCR under 2.5 mm radial compression.

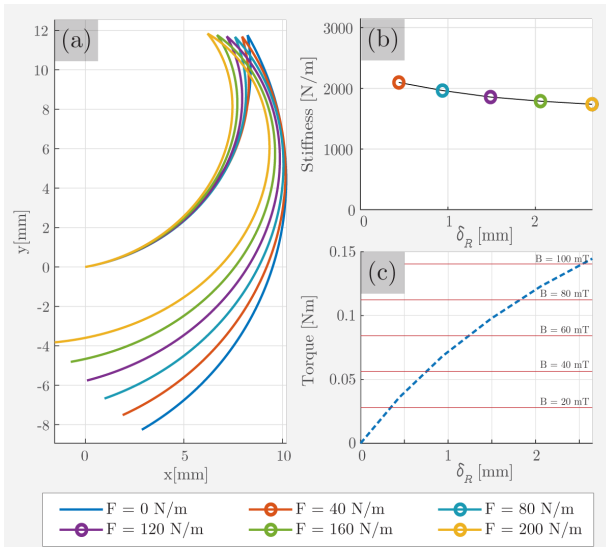


Figure 6: Results of stiffness modeling of flexure pairs. (a) Shapes of the 1.50-scale flexure-pairs under increasing load. (b) Stiffness of the flexure pair under increasing deformation. (c) Comparison of stall torque due to friction under increasing radial deformation and maximum torque produced by a magnetic field.

## 5 Prototype Experiments

Experiments are performed on prototypes of the CMCR to provide a proof-of-concept of its function (**Please refer to the supplementary video**). The movability and radial adaptability of the CMCR is tested within a test-setup with a handheld magnet and with the BigMag system [32]. Some additional experiments are performed to test the rest of the functionality of the CMCR.

### 5.1 Motion Experiments

The movement capabilities of the CMCR are tested in acrylic tubes of different shapes. The rotational external field in these experiments is created with a handheld Ø60 mm N42 disc magnet (Model S-60-05-DN, Supermagnete, Gottmadingen, Germany) which is rotated around the acrylic tubes. The 1.00-scale prototype is used in these motion experiments to show the capabilities at the intended clinically relevant scale. The experiments are performed without compressing the CMCR's flexure-pairs, meaning at the default diameter of the device.

The acrylic tubes used in these experiments all are manufactured from the same straight transparent acrylic tube with an inner diameter (ID) of 21 mm (Acrylic Tube Transparent 25x2 mm, Kunststofshop.nl, Zevenaar, The Netherlands). Two tubes with different curves have been fabricated by heating the tube with a heat gun and gradually bending them. One tube has a S-shape with two relatively sharp 30° curves and the other tube has a gradual 50° curve. Besides these two tubes, a straight tube is used to test straight movement. Silicone spray (Valvoline, Lexington, KY, USA) is applied to the tubes right before the experiments to provide some lubrication between the tubes and the prototype.

Results of these movement experiments can be found in Fig. 7. The internal magnetic field of the capsule robot aligns with the external field in the experiments. Rotation of the CMCR is observed when rotating the external magnet around the tubes. In addition, forward and backward movement occurs in all tubes when rotating the external magnet slightly in front or behind the capsule robot. This applies to the straight tube (Fig. 7a) as well as the curved tubes (Fig. 7b and Fig. 7c). Movement of the external magnet along the tubes without rotating around the tubes resulted occasionally also in forward and backward slipping of the CMCR.

### 5.2 Radial Adaptability Experiments

The radial adaptability of the CMCR is tested in acrylic tubes with different inner diameters. The focus of these experiments was to evaluate the straight movement of the capsule robot when the

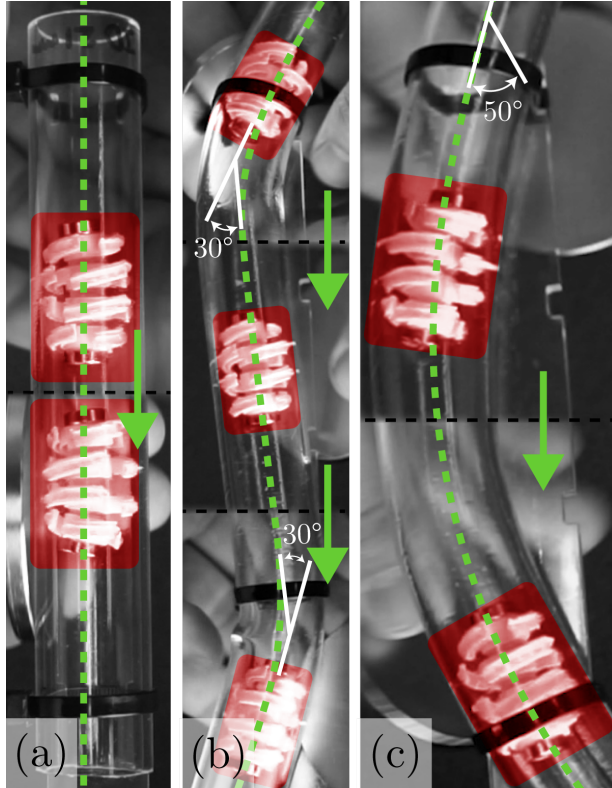


Figure 7: Results of the motion experiments with a handheld disc magnet. 1.00-scale prototype (uncompressed) in acrylic tubes with inner diameter 21 mm in: (a) straight motion, (b) 2x30° S-shape motion, and (c) 50° curved motion. All images are frames of the recorded videos of the experiments with the line of movement visualized (green dotted line) and the uncompressed capsule robot indicated (red box).

flexure-pairs are uncompressed or compressed. Both 1.25-scale and 1.50-scale prototypes are tested in these experiments. The rotational external magnetic field is obtained with the previously used handheld Ø60 mm disc magnet.

Testing of the uncompressed prototype is performed in straight acrylic tubes with relatively large inner diameters equal to the default diameters of the prototypes. Experiments with the compressed prototype are performed in straight acrylic tubes with relatively small inner diameters which are 5 mm smaller than the default diameters of the prototypes. This means that the 1.25-scale prototype is tested in respectively ID26 mm and ID21 mm tubes. The 1.50-scale prototype is tested in tubes with respectively ID32 mm and ID26 mm. Silicone spray is applied to all tubes right before testing to provide lubrication between the tubes and the prototype.

Fig. 8a and Fig. 8b show the results of the experiments with the 1.25-scale prototype as an example of these experiments. The internal magnetic dipole of the prototypes aligns in all experiments with the external magnetic field of the handheld magnet

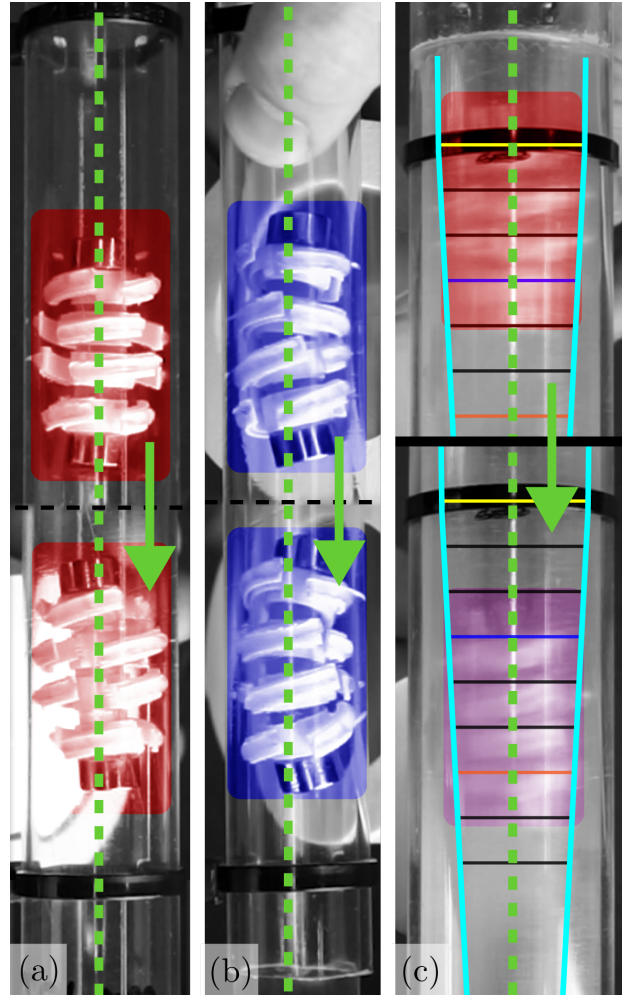


Figure 8: Results of the radial adaptability experiments with a handheld disc magnet and the 1.25-scale prototype. (a) The uncompressed prototype in an ID26mm tube (red boxes) and (b) compressed prototype in an ID21mm tube (blue boxes). (c) Radial adaptability experiment of the capsule robot from an uncompressed state (red box) up to a partly compressed state (purple box) in a tapered tube with ID26-21mm (light blue lines). All images are frames of the recorded videos of the radial adaptability experiments and show movement over the visualized line of movement (green dotted line).

around the tubes. The CMCR is slightly bent in the axial direction by the external magnetic field. Rotational, backward, and forward movement was observed in both prototypes during the uncompressed and compressed fixed inner diameter experiments.

A tapered tube is tested besides the fixed diameter experiments. This is done to analyze the behavior of the CMCR during an inner diameter change of the tube. A flexible tapered tube with ID26 mm to ID21 mm over a distance of 100 mm is printed with Elastic 50A Resin in the Forms 2 SLA printer. This flexible tube is glued into an acrylic transparent

tube with ID32 mm. The inner surface of the flexible tapered tube is covered with silicone spray to lubricate the surface between the tube and the prototype. The prototype is moved from the large inner diameter side to the small inner diameter side of this tube.

Both rotational and forward movement of the CMCR is noticed during this experiment. However, both rotational and forward movement is obstructed halfway the tapered tube during the experiment with this tube (Fig. 8c). The capsule robot is partly compressed at that point. The robot is released from this tapered tube by rotating and moving the external magnetic field in the opposite direction.

### 5.3 BigMag System Motion Experiments

The BigMag system [32] is used to repeat some of the previously presented experiments with acrylic tubes. The magnetic field of the BigMag system replaces the handheld magnet in the previous experiments. These experiments are performed to examine the functionality of the CMCR in an uniform external magnetic field.

In Fig. 9a some results of experiments are presented. The internal magnetic dipole of the prototypes aligns with the external magnetic field created by BigMag. Rotational and forward movement is observed in both compressed and uncompressed experiments with the acrylic tubes. An external magnetic field of approximately 50 mT is applied during the compressed experiments to achieve movement, and a field of approximately 10 mT during the uncompressed experiments. No axial bending of the capsule robot is visible in all these experiments.

In addition to these solid acrylic tubes, softer tubes are manufactured to test the CMCR in another environment. The inside of two acrylic tubes is coated with 5 mm gelatin to create these softer tubes. The gelatin is made by adding 6% w/w chemical-grade gelatin (Gelatin powder, Dr. Oetker, Bielefeld, Germany) to distilled water. Closed cylinders with an 5 mm smaller radius than the acrylic tubes are 3D printed as molds for the gelatin coating. These cylinders are covered with mold release spray and inserted in the acrylic tubes. The liquid gelatin is poured in the space between the cylinders and the tubes. The cylinders are removed from the tubes after overnight hardening of the gelatin. This resulted in two gelatin-coated tubes with inner diameters of 26 mm and 21 mm. Uncompressed and compressed experiments with the 1.25-scale prototype are done with these gelatin-coated tubes.

Rotational and forward movement without damage is observed in the experiment with the gelatin-coated ID26 mm tube, as can be seen in Fig. 9b. Nevertheless, only rotational movement is found in the smaller gelatin-coated ID21 mm tube. The CMCR was partly compressed in this experiment and

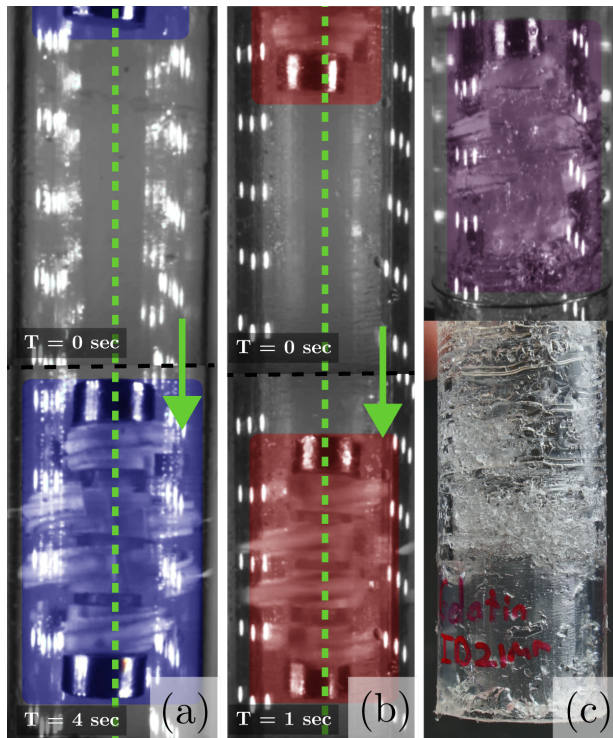


Figure 9: Results of the experiments with the BigMag system: (a) The compressed 1.50-scale prototype (blue boxes) pulled over the line of movement (green dotted line) into the magnetic center of the 10 mT external rotational magnetic field of BigMag in a acrylic ID26 mm tube. (b) The uncompressed 1.25-scale prototype (red boxes) pulled into the magnetic center of the 50 mT external rotational magnetic field of BigMag system in a gelatin-coated ID26mm tube. (c) The partly compressed 1.25-scale prototype (purple box) ruining the gelatin coating of the gelatin-coated ID21 mm tube while rotating due to the external magnetic field of BigMag (top), and the tube with the ruined gelatin coating (bottom).

the gelatin was damaged by the robot (Fig. 9c). In all experiments with BigMag no axial bending of the capsule robot is visible (Fig. 9).

### 5.4 Additional Experiments

Besides the previously described experiments, two additional experiments are performed to test the CMCR in more clinically relevant settings. The handheld Ø60 mm disc magnet is used for the external magnetic field in both experiments.

Since the intended application is cardiovascular interventions, the motion of the CMCR in flowing liquid is the focus of the first additional experiment. Water with red dye is used as the liquid, and an ID21 mm tube is connected to a peristaltic pump (MCP ISM404 pump with a Pro-380 ISM791 pump head, Ismatec®, Wertheim, Germany) that cycles the water at 2.9 L/min. The 1.00-scale prototype is

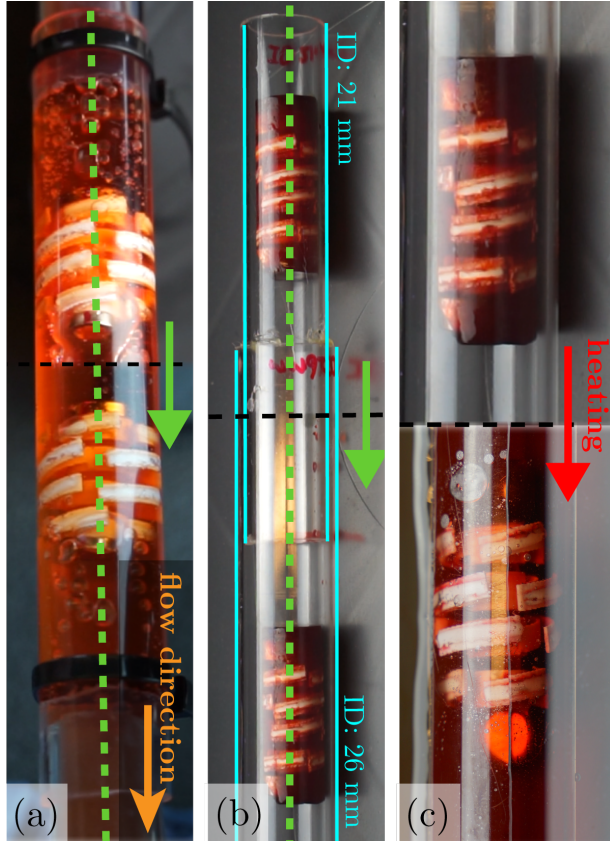


Figure 10: Results of the additional experiments. (a) Motion test of the 1.00-scale prototype in the fluid flow. (b) Insertion of the compressed 1.25-scale CMCR encapsulated in ice from ID21 mm tube to ID26 mm tube. (c) Releasing CMCR from ice using warm water to expand to 26 mm.

tested in this setup in uncompressed state (Fig. 10a). The CMCR holds steady in the flowing water, and only moves when the rotating magnetic field is applied. Additionally, it does not block the flow of liquid.

The second additional experiment is performed to demonstrate an approach for minimally invasive insertion of the CMCR. The 1.25-scale prototype is fully compressed and embedded in a block of ice with an outer diameter of approximately 20 mm. An ID21 mm acrylic tube is glued to a larger ID26 mm acrylic tube. The prototype embedded in ice is then inserted through the small tube and guided to the larger tube using the magnet (Fig. 10b). Once at the target location in the large tube, the ice capsule is melted with warm water, which releases the flexures and causes the CMCR to anchor in place within the larger tube (Fig. 10c).

## 6 Discussion

In this study the design of a compliant magnetic capsule robot is presented and tested. An evaluation

of the design requirements (Sec. 2) for the CMCR is given in Table 3. Except requirement R5, the CMCR meets all requirements. The radial elastic modulus of CMCR (requirement R5) cannot be confirmed with the research in this report and should be tested and optimized more. Nevertheless, the experimental results show that the CMCR is able to move through acrylic tubes when uncompressed (Fig. 7) and compressed (Fig 8), and through gelatin-coated tubes when uncompressed (Fig. 9b). This indicates a sufficient radial stiffness/ elastic modulus of the CMCR.

Straight and curved movement is found in most uncompressed and compressed experiments. Even though the rotation of the robot sometimes seemed less steady in compressed tests than in the uncompressed tests, no problems occurred in the compressed experiments with solid acrylic tubes (Fig. 8a and Fig. 8b). However, problems did arise in the experiments with the ID21 mm gelatin-coated tube (Fig. 9c) and the tapered flexible tube (Fig. 8c). The gelatin coating is damaged by the CMCR due to high stiffness of flexures compared to the gelatin, and stagnation of the movement of the robot is seen in the tapered elastic resin tube due to high friction between the CMCR and the elastic resin. Low compliance to the surrounding environment, high stiffness and/or surface roughness of the CMCR could cause these problems. More optimization of these robot properties by changing materials and dimensions could solve this. On the other hand, the problems could be due to the test setups since both the gelatin-coated tube and tapered tube do not fully replicate a blood vessel. This means that realistic blood vessel phantoms should be used when optimizing the robot properties.

Forward and backward slipping is sometimes observed in both compressed and uncompressed experiments when the external magnet is moving along the tubes without rotating. On the other hand, no noticeable slipping of the CMCR in flowing liquid (Fig. 10a) indicates that slipping might not be a problem. Experiments in more realistic blood vessel phantoms could help to conclude on this matter and optimize the friction between the CMCR and the environment. Different clinically relevant actuation systems such as the ARMM system [33] could be used for these tests. The successfully-tested minimally invasive insertion approach (Fig. 10b and Fig. 10c) can be used in these clinically relevant tests.

Three different scales of prototypes are used to test the performance of the CMCR with respect to the flexure-stiffnesses since the in-house 3D printers limited the stiffness of the 1.00-scale prototype. The 1.00-scale prototype is clinically relevant since it fits in the abdominal aorta. However, the other scale (1.25 $\times$  and 1.50 $\times$ ) are not. Even though these three different scales are sufficient to demonstrate a proof-of-concept of the functionality of the CMCR,

Table 3: Evaluation of the design requirements of the compliant magnetic capsule robot (CMCR).

| Requirements   | Implemented  | Score |
|--|--|-------|
| R1 $d_0^r <^\epsilon d_a \rightarrow d_{r,0} \approx 21$ mm [22, 23] | $d_0^r = 21$ mm  | 3/3   |
| R2 $d_r = d_0^r - \delta_a$ where $\delta_a > 2.3$ mm                | $d_r = 17$ mm with $\delta_r = 4$ mm   | 3/3   |
| R3 Magnetically-actuated movement                                    | Movement is magnetically-actuated  | 3/3   |
| R4 $\alpha_c = 50^\circ$ with $L_c = 70$ mm                          | CMCR moves through sharp $30^\circ$ curves   | 2/3   |
| R5 Biocompatible,<br>$E_r \approx E_a \in [0.1, 1]$ MPa              | More research is necessary to conclude on this requirement.  | 1/3   |
| R6 $A_r < 0.7A_a$  | $A_r \approx 20$ mm <sup>2</sup> and $A_a \approx 63$ mm <sup>2</sup> , so<br>$A_r \approx 0.3A_a$ | 3/3   |
| R7 $Q_a = 2.9 \pm 0.6$ L/min   | CMCR performs in $Q_a = 2.9$ L/min   | 2/3   |

the flexure-stiffness of the 1.00-scale prototype should be optimized. Using different (external) fabrication methods or replacing the ABS material could optimize this stiffness. This optimization will get rid of the need for these different scales of prototypes.

Unintended axial bending of the CMCR occurs in some tests with the less controlled external magnetic field of the handheld magnet (Fig. 8a and Fig. 8b). A controlled uniform external magnetic field like the field of the BigMag system solves this problem ((Fig. 9a and Fig. 9b). Nevertheless, this axial bending indicates possible improvements for the CMCR. Improving the magnetic design of the CMCR could advance the robot by integrating the magnets in the robot instead of on the ends of the robot. Besides this, the pill-like shape due to the flexure-pairs segments with two different diameter is probably irrelevant for the radial adaptability. The use of three equal diameter flexure-pair segments would probably be sufficient and would also improve the axial stability of the CMCR since this will increase the contact surface with the blood vessel.

Besides the design and prototypes, a mathematical model for the flexure-stiffness is presented in this research. The maximum required magnetic field of 50 mT (Fig. 6c) is in accordance to the applied field in the BigMag experiments (Fig. 9). Even though this seems to validate the model, more validation of the flexure-pair stiffness calculation of the model could be performed. The distributed force on the outer flexure is also doubtful since realistically more force is acting during radial compression on the side where flexures are connected. Both these concerns should be evaluated in future work with e.g. experiments and finite element methods.

## 7 Conclusions & Future Work

The CMCR presented in this research is a combination of continuum flexures, compliant parts, and permanent magnets. The uncompressed CMCR moves through curved and straight tubular structures

by untethered actuation of a rotational external magnetic field. In addition, the CMCR moves under radial compression in straight tubular structures with different diameters. Although the CMCR shows favorable functionality, optimization of the robot should be done in realistic blood vessel phantoms to obtain optimal compliance, stiffness, and surface-smoothness. A foundation for this optimization is offered by the design, the results, and flexure-pair model in this report.

Besides this, the movability of the CMCR by magnetic actuation demonstrates a proof-of-concept for untethered robotic possibilities for cardiovascular surgical interventions. The radial adaptability by passive elements expands this to a proof-of-concept of hybrid passive-active robots for this application. The MIS insertion with ice shows a clinically relevant approach to use the CMCR in clinics. Therefore, the capsule robot presented in this research is a first step toward untethered surgical intervention tools. Although some insights in this field of research are found by this study, more studies are required before a market ready robot can be produced.

Future work could focus on optimizing the CMCR with respect to stiffness and surface-smoothness in realistic blood vessel phantoms to discover more insights in the use of these type of capsule robots. In addition, surgical interventions tools should be designed and added to the CMCR for a more extensive proof-of-concept of these untethered surgical intervention tools. Furthermore, different approaches for these untethered tools could and should be explored to find the most optimal approach.

## References

- [1] J.E.A. Wickham. Minimally Invasive Surgery. *Journal of Endourlogy*, 1(2):71–74, 1987.
- [2] B. Jaffray. Minimally invasive surgery. *Arch Dis Child*, 90:537–542, 2005.
- [3] R.A. Beasley. Medical Robots: Current Systems and Research Directions. *Journal of Robotics*, 2012:1–14, 2012.
- [4] V. Vitiello, S.L. Lee, T.P. Cundy, and G.Z. Yang. Emerging robotic platforms for minimally invasive surgery. *IEEE Reviews in Biomedical Engineering*, 6:111–126, 2013.
- [5] J. Burgner-Kahrs, D.C. Rucker, and H. Choset. Continuum Robots for Medical Applications: A Survey. *IEEE Transactions on Robotics*, 31(6):1261–1280, Dec. 2015.
- [6] M. Sitti, H. Ceylan, W. Hu, J. Giltinan, M. Turan, S. Yim, and E. Diller. Biomedical Applications of Untethered Mobile Milli/Microrobots. *Proceedings of the IEEE*, 103(2):205–224, 2015.
- [7] T.L. Thomas, V.K. Venkiteswaran, G.K. Ananthasuresh, and S. Misra. Surgical Applications of Compliant Mechanisms: A Review. *Journal of Mechanisms and Robotics*, 13(2):020801, 2021.
- [8] M. Runciman, A. Darzi, and G.P. Mylonas. Soft Robotics in Minimally Invasive Surgery. *Soft Robotics*, 6(4):423–443, 2019.
- [9] C. Bedell, J. Lock, A. Gosline, and P.E. Dupont. Design optimization of concentric tube robots based on task and anatomical constraints. *Proceedings - IEEE International Conference on Robotics and Automation*, pages 398–403, 2011.
- [10] S. Jeon, A.K. Hoshiar, K. Kim, S. Lee, E. Kim, S. Lee, J. Kim, B.J. Nelson, H. Cha, B. Yi, and H. Choi. A Magnetically Controlled Soft Microrobot Steering a Guidewire in a Three-Dimensional Phantom Vascular Network. *Soft Robotics*, 6(1):54–68, 2019.
- [11] B.J. Nelson, I.K. Kaliakatsos, and J.J. Abbott. Microrobots for Minimally Invasive Medicine. *Annual Review of Biomedical Engineering*, 12(1):55–85, 2010.
- [12] G. Iddan, G. Meron, A. Glukhovsky, and P. Swain. Wireless capsule endoscopy. *Nature*, 405(6785):417–418, May 2000.
- [13] A.M. Singeap, C. Stanciu, and A. Trifan. Capsule endoscopy: The road ahead. *World Journal of Gastroenterology*, 22(1):369–378, Jan. 2016.
- [14] G. Ciuti, R. Caliò, and D. et al. Camboni. Frontiers of robotic endoscopic capsules: a review. *Journal of Micro-Bio Robotics*, 11(1-4):1–18, Jun. 2016.
- [15] A.J. Zhao, Y.Y. Qian, H. Sun, X. Hou, J. Pan, X. Liu, W. Zhou, Y.Z. Chen, X. Jiang, Z.S. Li, and Z. Liao. Screening for gastric cancer with magnetically controlled capsule gastroscopy in asymptomatic individuals. *Gastrointestinal Endoscopy*, 88(3):466–474, Sep. 2018.
- [16] S. Yim, E. Gultepe, D.H. Gracias, and M. Sitti. Biopsy using a magnetic capsule endoscope carrying, releasing, and retrieving untethered microgrippers. *IEEE Transactions on Biomedical Engineering*, 61(2):513–521, 2014.
- [17] D. Son, H. Gilbert, and M. Sitti. Magnetically Actuated Soft Capsule Endoscope for Fine-Needle Biopsy. *Soft Robotics*, 7(1):10–21, 2020.
- [18] Lan N. Pham, Jake A. Steiner, Kam K. Leang, and Jake J. Abbott. Soft Endoluminal Robots Propelled by Rotating Magnetic Dipole Fields. *IEEE Transactions on Medical Robotics and Bionics*, 2(4):598–607, 2020.
- [19] I.S.M. Khalil, A. Adel, D. Mahdy, M.M. Micheal, M. Mansour, N. Hamdi, and S. Misra. Magnetic localization and control of helical robots for clearing superficial blood clots. *APL Bioengineering*, 3:026104, 2019.

- [20] Katie M. Popek, Thomas Schmid, and Jake J. Abbott. Six-Degree-of-Freedom Localization of an Untethered Magnetic Capsule Using a Single Rotating Magnetic Dipole. *IEEE Robotics and Automation Letters*, 2(1):305–312, 2017.
- [21] V.K. Venkiteswaran, D.K. Tan, and S. Misra. Tandem actuation of legged locomotion and grasping manipulation in soft robots using magnetic fields. *Extreme Mechanics Letters*, 41:101023, 2020.
- [22] A.T. Hirsch, Z.J. Haskal, N.R. Hertzner, and C.W. Bakal et al. ACC/AHA 2005 practice guidelines for the management of patients with peripheral arterial disease (Lower extremity, renal, mesenteric, and abdominal aortic). *Circulation*, 113(11):e463–e654, 2006.
- [23] H. Silaghi, A. Branchereau, S. Malikov, and Aurel Andercou. Management of small asymptomatic abdominal aortic aneurysms—a review. *International Journal of Angiology*, 16(4):121–127, Sep. 2007.
- [24] T. Xu, J. Yu, X. Yan, H. Choi, and L. Zhang. Magnetic Actuation Based Motion Control for Microrobots: An Overview. *Micromachines*, 6(9):1346–1364, 2015.
- [25] M. Boufi, C. Guivier-Curien, A.D. Loundou, V. Deplano, O. Boiron, K. Chaumoitre, V. Gariboldi, and Y.S. Alimi. Morphological Analysis of Healthy Aortic Arch. *European Journal of Vascular and Endovascular Surgery*, 53(5):663–670, 2017.
- [26] T. Khamdaeng, J. Luo, J. Vappou, P. Terdtoon, and E.E. Konofagou. Arterial stiffness identification of the human carotid artery using the stress-strain relationship in vivo. *Ultrasonics*, 52(3):402, Mar. 2012.
- [27] E. Good, T. Länne, E. Wilhelm, J. Perk, T. Jaarsma, and E. de Muinck. High-grade carotid artery stenosis: A forgotten area in cardiovascular risk management. *European journal of preventive cardiology*, 23(13):1453–1460, Sep. 2016.
- [28] C.A. Taylor, C.P. Cheng, L.A. Espinosa, B.T. Tang, D. Parker, and R.J. Herfkens. In vivo quantification of blood flow and wall shear stress in the human abdominal aorta during lower limb exercise. *Annals of Biomedical Engineering*, 30(3):402–408, 2002.
- [29] L. Yang, X. Du, E. Yu, D. Jin, and L. Zhang. DeltaMag: An electromagnetic manipulation system with parallel mobile coils. *Proceedings - IEEE International Conference on Robotics and Automation*, 2019-May:9814–9820, May 2019.
- [30] J. Nam, W. Lee, J. Kim, and G. Jang. Magnetic helical robot for targeted drug-delivery in tubular environments. *IEEE/ASME Transactions on Mechatronics*, 22(6):2461–2468, Dec. 2017.
- [31] V.K. Venkiteswaran and H.J. Jun Su. Pseudo-rigid-body models for circular beams under combined tip loads. *Mechanism and Machine Theory*, 106:80–93, 2016.
- [32] J. Sikorski, I. Dawson, A. Denasi, E.E.G. Hekman, and S. Misra. Introducing BigMag - A novel system for 3D magnetic actuation of flexible surgical manipulators. *Proceedings - IEEE International Conference on Robotics and Automation*, pages 3594–3599, Jul. 2017.
- [33] J. Sikorski, C.M. Heunis, F. Franco, and S. Misra. The ARMM system: An optimized mobile electromagnetic coil for non-linear actuation of flexible surgical instruments. *IEEE Transactions on Magnetics*, 55(9), Sep. 2019.
- [34] T.L. Thomas, V.K. Venkiteswaran, G.K. Ananthasuresh, and S. Misra. A Monolithic Compliant Continuum Manipulator: A Proof-of-Concept Study. *Journal of Mechanisms and Robotics*, 12(6), Dec. 2020.

# Appendices

## A Design & Design Process

A systematic design approach is used to design the untethered capsule robot. The design process and the choices made for this capsule robot is elaborated in this appendix.

### A.1 Design Objective

The original objective of this research is an untethered minimally invasive surgical intervention tool for tubular structures. The abdominal aorta emerged from background research as a suitable structure given the available design space and the cardiovascular focus of the Surgical Robotics Lab (SRL). Some surgical interventions within this structure were considered to find the possibilities for an intervention tool. Stent placement seemed to be a reasonable aim since the required intervention motion is in the radial direction of the artery. The original objective converged by combining it with these remarks to an untethered stent placing capsule robot for the abdominal aorta.

### A.2 Objective Adjustment

The objective of this untethered stent placement capsule robot was adjusted later in the project to a compliant magnetic capsule robot due to the time-limitation of the project. The design process in this appendix is described with the focus on the previously mentioned objective. The compliant magnetic capsule robot is basically an intermediate step towards untethered capsule robots such as an untethered stent placement capsule robot.

### A.3 Requirements & Constraints

The requirements and constraints for the stent placement capsule robot were drafted through an iterative process. This resulted in the following quantified requirements and constraints which provided some guidelines throughout the design process:

#### Requirements:

- The device should place a cardiovascular stent properly and accurately at the predefined position. (*weight: 4*)
- The device should provide 50Hz position feedback with a resolution of 0.1 mm. (*weight: 4*)
- The device should provide 50Hz feedback of the intervention process. (*weight: 4*)
- The device should be able to passively adapt its diameter to  $\pm 20\%$  of its default diameter. (*weight: 4*)

#### Constraints:

- The device should be manipulated with magnetic actuation within a range of 1 mm from the target position [35]. (*weight: 3*)
- The device should have a minimum diameter of  $\leq 18$  mm. (*weight: 3*)
- The device should match the compliance of aortic tissue when making contact. (*weight: 3*)
- The device should be able to bend of  $25^\circ$  over an arch length of 35 mm [36]. (*weight: 3*)
- The device should not block more than 70% of the surface of a blood vessel's cross section. (*weight: 3*)
- The device should be controlled wirelessly within a 30-50 mT magnetic field in the lab environment. (*weight: 3*)
- The device should not be limited in movement by vessel narrowing due to (e.g.) plaques. (*weight: 2*)
- The device should function within the  $2.9 \pm 0.6$  L/min blood flow in the abdominal aorta at rest [37]. (*weight: 2*)
- The device should be biocompatible. (*weight: 2*)
- The device should be able to perform the complete intervention within 1 hour. (*weight: 2*)
- The device should be inserted in and extracted from the arteries minimally invasively. (*weight: 2*)
- The device should be scalable. (*weight: 2*)



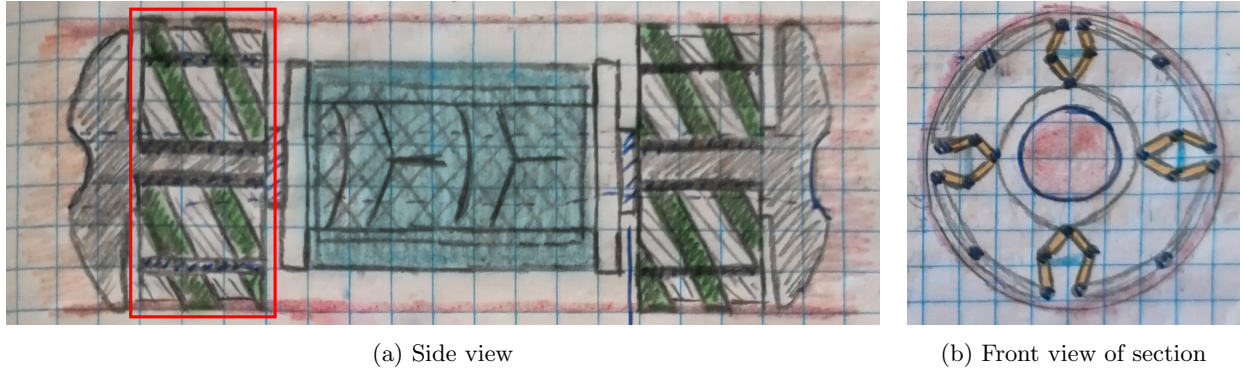


Figure A.2: An example of a hand sketch of a full system concept: (a) Side view of the concept with a helix for movement (green) and a biodegradable stent capsule (blue), (b) Front view of the section which highlighted by the red box in (a), showing origami-based flexures for radial flexibility, (orange).

this selection gave some results. No hard conclusions could be drawn on these results due to this subjectivity. Despite this insignificance, the results could be used to attain some perception on how to advance.

Some basic experiments were performed on the precepts to objectively assess them and to give some insights for design choices in the final design. Although the conceptual design already contained full system concepts, the tests were carried out on the functional precepts to continue the process in a systematic and modular way. All the executed tests consisted of manufacturing prototypes of some precepts for a specific function and testing these prototypes. The following test were done for: movement (Section A.6.1), passive radial flexibility (Section A.6.2), and passive axial flexibility (Section A.6.3).

### A.6.1 Movement

The millipede movement precept seemed — while reviewing the precepts — to be the most feasible concept. This concept is based on the millipede design of Venkiteswaran et al. [38]. Two of these millipedes are connected to the opposite sides of a capsule. The magnetized legs of the millipedes move by rotating an external magnetic field around their side axis. By connecting these millipedes to a core, the device could in theory walk to the target position through the leg movement.

Besides this concept, another movement concept arose during the precept review. This concept uses a screw-like helical shape to move the device by rotating. Yang et al. amongst others used the same principle in their research [39]. The rotational actuation can be achieved by magnetizing the device and rotating an external magnetic field around the longitudinal axis of the device.

Prototypes of these two concepts are designed, manufactured, tested and improved iteratively until some reasonable conclusions could be drawn from the test results. The prototypes are manufactured by molding, 3D-printing with the Stratasys Fortus 250mc, magnetizing and assembling (see Fig. A.3). Different soft materials are tested for the helical threads and the millipedes. The rotational external magnetic fields for the tests are generated by hand with some powerful permanent magnets and the BigMag system in the SRL [40].

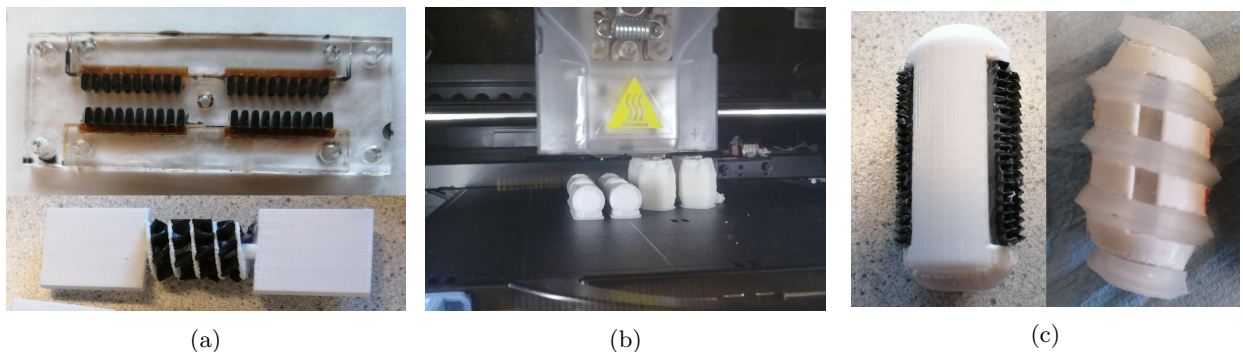


Figure A.3: Overview of manufacturing and assembling of movement prototypes: (a) Millipede molding (top) and millipede magnetization tool (bottom), (b) 3D printing in the Stratasys Fortus 250mc, and (c) assembled millipede-based (left) and helical thread-based prototype (right)

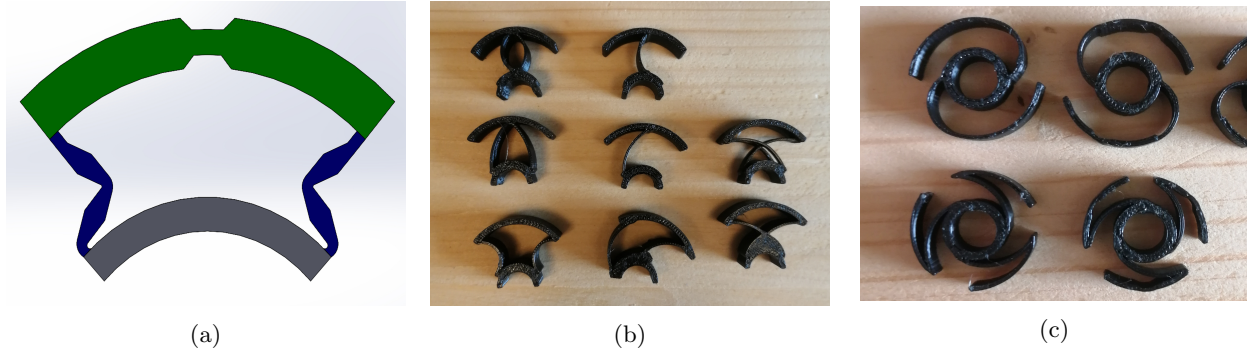


Figure A.4: Overview of different versions of the passive radial flexibility concept: (a) Initial concept with origami-based elastic elements (blue), outer cylinder (green) and inner core (grey), (b) multiple 3D printed leaf spring configurations, and (c) final tested full radius flexibility concepts

The silicone (Ecoflex™00-10, Smooth-On, Inc., USA) millipede legs seemed to lack rigidity to carry the weight of the 3D printed capsule. For this reason, millipedes of a more rigid rubber (PMC™-770, Smooth-On, Inc., USA) were tried. However, the flexibility of this material was insufficient to achieve proper movement of the millipede legs. A proper material with enough weight carrying capacity and flexibility could have been found with some more material testing. Nevertheless, it was concluded that this might only work for the test setup for this single function. The millipede might be unable to move in the full system since the legs will be pressed against the surrounding tissue wall when considering the radial passive adaptability function. From this thought the conclusion emerged that this preconcept is not reliable to use in the design of the full system.

The helical concept on the other hand showed some promising results. The prototypes were able to move in the longitudinal direction if and only if it was rotating. Besides, they only seemed to move in the longitudinal direction due to the pull of the external magnetic field and not due to forces on the helix as expected. Nevertheless, this pull can easily be achieved by just making some changes to the external actuation. It was concluded with these properties in mind to move forward with this preconcept.

### A.6.2 Passive Radial Flexibility

The main idea for this function was already in the conceptual design to have a relatively rigid inner core and a flexible outer structure which are connected through some sort of elastic element. The passivity could be attained by manufacturing these segments in the maximum diameter since certain materials want to go back to the original shape when compressed to a smaller diameter. The review of the function's preconcepts however concluded that none of the preconcepts were sufficient and feasible to achieve this idea.

Another concept was drafted given the lack of a proper concept at this point in the process. This concept (see Fig. A.4a) is a combination of inspiration from origami and some other preconcepts. Some thicker, more rigid segments and some thinner, more flexible segments — like seen in origami-based designs — formed the elastic element of the concept. The relative simplicity and theoretical proper functioning made this a suitable design. Nevertheless, the manufacturability of this idea was poor given the dimension of the design and the possibilities within the SRL. As a result of this, the design was simplified.

This simplification was done by changing the elastic segments to leaf springs. Multiple leaf spring configurations (see Fig. A.4b) were tried by 3D printing and testing them by hand. Observations within these trials were used to draft optimized concepts for this function (see Fig. A.4c). The design was concluded through a simple range test by hand to be sufficient and feasible for in a full system concept.

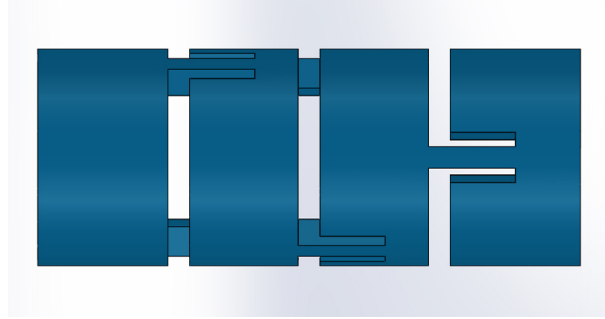
### A.6.3 Passive Axial Flexibility

Axial flexibility is needed in the capsule robot to enable the robot to move through curves in the abdominal aorta. Axial flexibility should be implemented in a cylindrical shape given the cylindrical shape of the capsule robot. The first concept of this flexible cylinder is based on flexible conduit. Different configurations of this concept are designed and 3D printed (Fig. A.5a). However, no flexibility is observed in all these concepts.

Another approach for axial flexibility of cylindrical shapes is found in literature [34]. A concept is elaborated based on this approach (Fig. A.5b). This concept is printed with several materials and flexure



(a)



(b)

Figure A.5: Overview of different concepts for axial flexibility: (a) flexible conduit based concept, and (b) flexure-based concept.

dimensions. Despite this, no optimal configuration is found since the flexures were too stiff or too fragile. The final concept for this axial flexibility is to make the cylindrical shape out of flexible material. This allows bending of the cylinder. Basic experiments with 3D printed flexible cylinders show axial flexibility of this concept. This led to the conclusion to move forward with this preconcept.

### A.7 Full system concept

The previously elaborated and selected precepts for the three subfunctions are merged into a concept for the capsule robot. The precepts are tuned in this process to enable this merging without the loss of functionality. Several prototypes of the capsule robot are iteratively fabricated to find the most optimal dimensions etc. The final prototype is shown in Fig. A.6.



Figure A.6: Prototype of the capsule robot

## Appendix References

- [35] A.D. Dwight, A. Elhaddi, K. Packard, V. Gupta, and T.A. Fischell. High Incidence of Inaccurate Stent Placement in the Treatment of Coronary Aorto-Ostial Disease. *Journal of Invasive Cardiology*, 23(8):322, 2011.
- [36] M. Boufi, C. Guivier-Curien, A.D. Loundou, V. Deplano, O. Boiron, K. Chaumoitre, V. Gariboldi, and Y.S. Alimi. Morphological Analysis of Healthy Aortic Arch. *European Journal of Vascular and Endovascular Surgery*, 53(5):663–670, 2017.
- [37] C.A. Taylor, C.P. Cheng, L.A. Espinosa, B.T. Tang, D. Parker, and R.J. Herfkens. In Vivo Quantification of Blood Flow and Wall Shear Stress in the Human Abdominal Aorta During Lower Limb Exercise. *Annals of Biomedical Engineering 2002 30:3*, 30(3):402–408, 2002.
- [38] V.K. Venkiteswaran, L.F.P. Samaniego, J. Sikorski, and S. Misra. Bio-inspired terrestrial motion of magnetic soft millirobots. *IEEE Robotics and Automation Letters*, 4(2):1753–1759, 2019.
- [39] L. Yang, X. Du, E. Yu, D. Jin, and L. Zhang. DeltaMag: An electromagnetic manipulation system with parallel mobile coils. *Proceedings - IEEE International Conference on Robotics and Automation*, 2019-May:9814–9820, May 2019.
- [40] J. Sikorski, I. Dawson, A. Denasi, E.E.G. Hekman, and S. Misra. Introducing BigMag - A novel system for 3D magnetic actuation of flexible surgical manipulators. *Proceedings - IEEE International Conference on Robotics and Automation*, pages 3594–3599, Jul. 2017.

## B Hand sketches of full system concepts

Many (hand) sketches have been made during the design process of the compliant magnetic capsule robot. For every subfunction (Section A.4) precepts have been sketched. These precepts are combined into full system concepts of which the hand sketches are presented in Fig. A.7, Fig. A.8 and Fig. A.9.

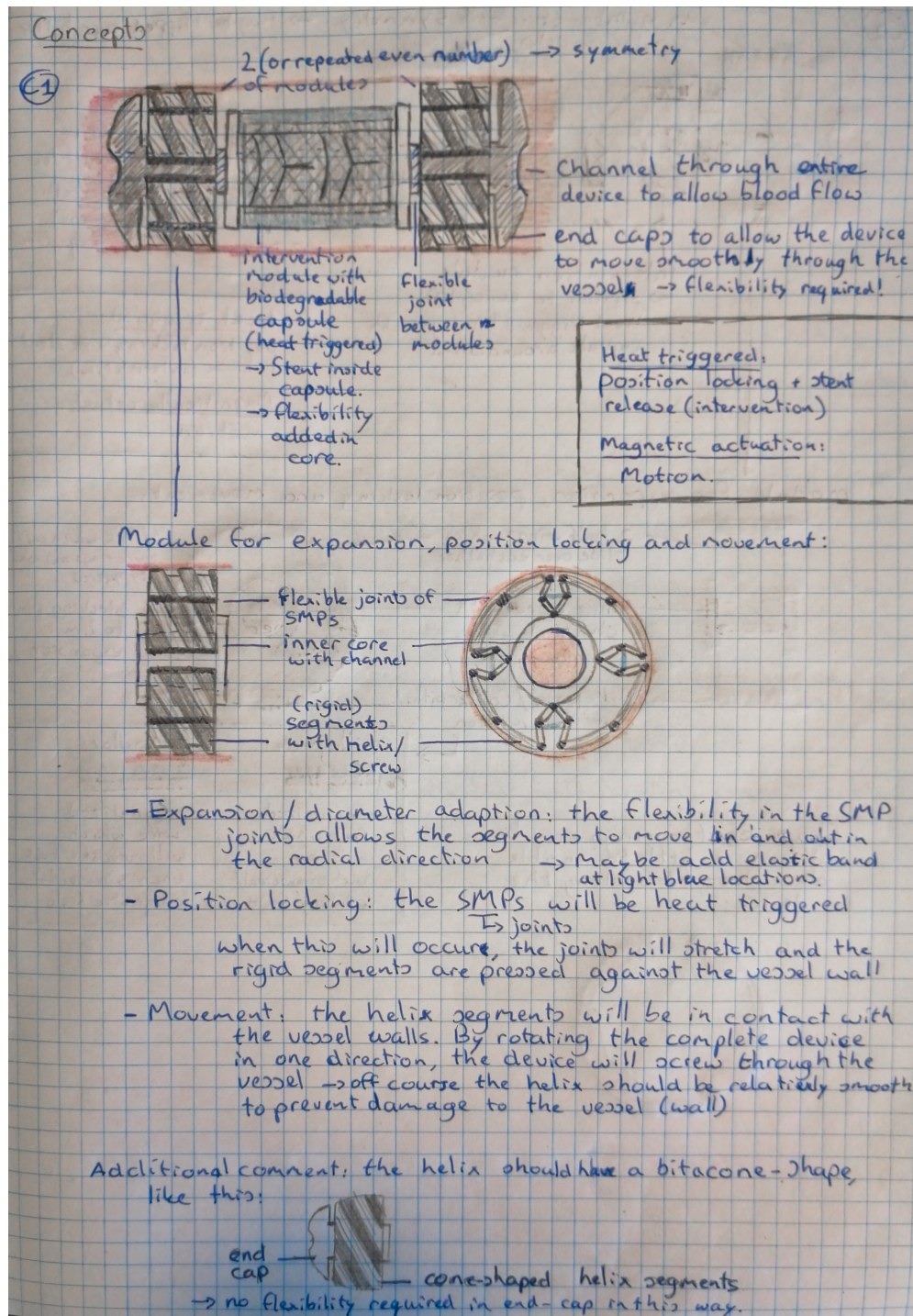


Figure A.7: Hand sketch of full system concept 1 with flexible parts for radial adaptation, Shape Memory Polymers (SMPs) for position locking, screw-like threads for movement, and biodegradable capsule for stent placement. See text on image for more explanation.

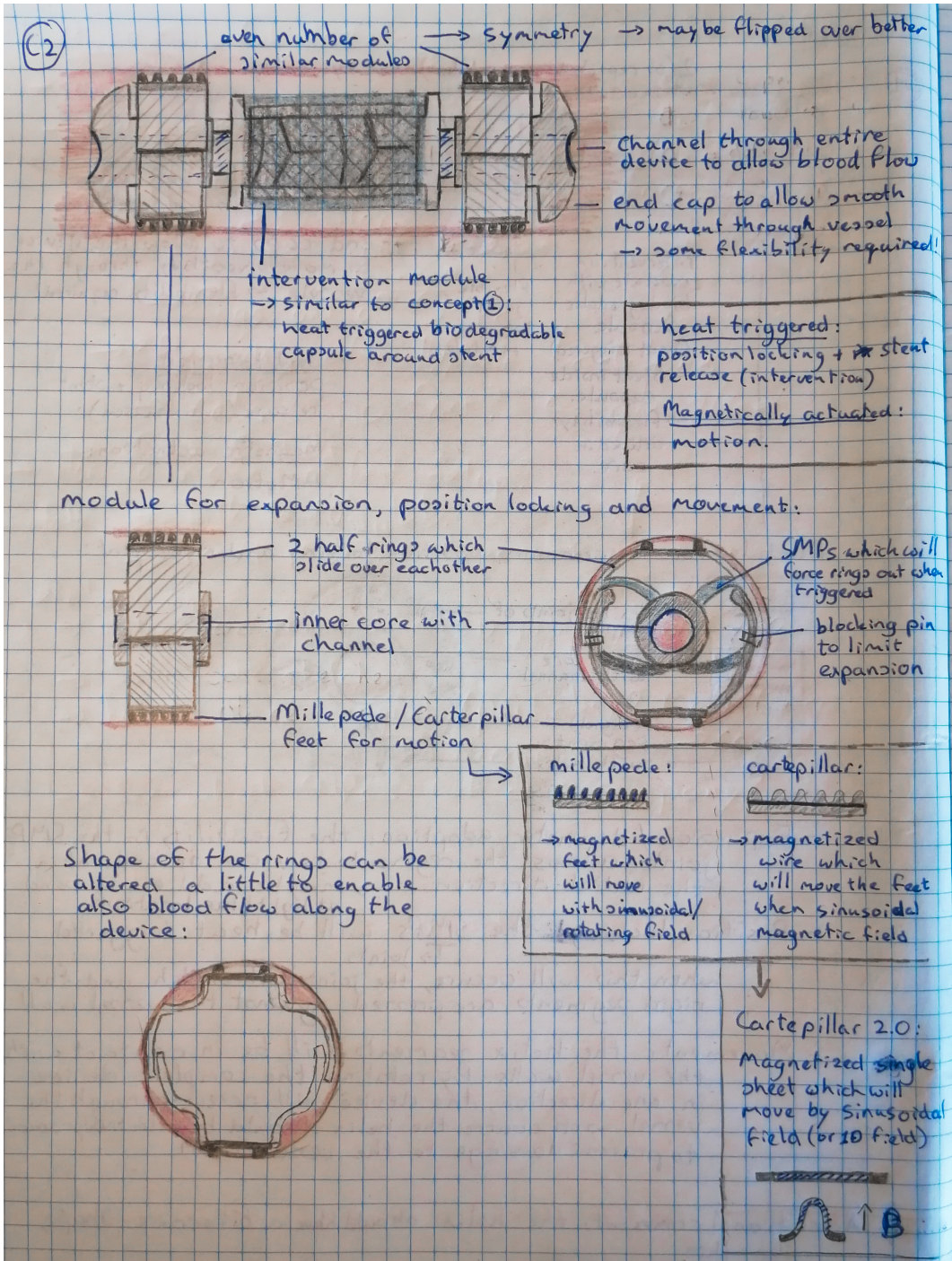


Figure A.8: Hand sketch of full system concept 2 with C-shaped rings and flexible parts for radial adaptation, Shape Memory Polymers (SMPs) for position locking, soft millipedes for movement, and biodegradable capsule for stent placement. See text on image for more explanation.

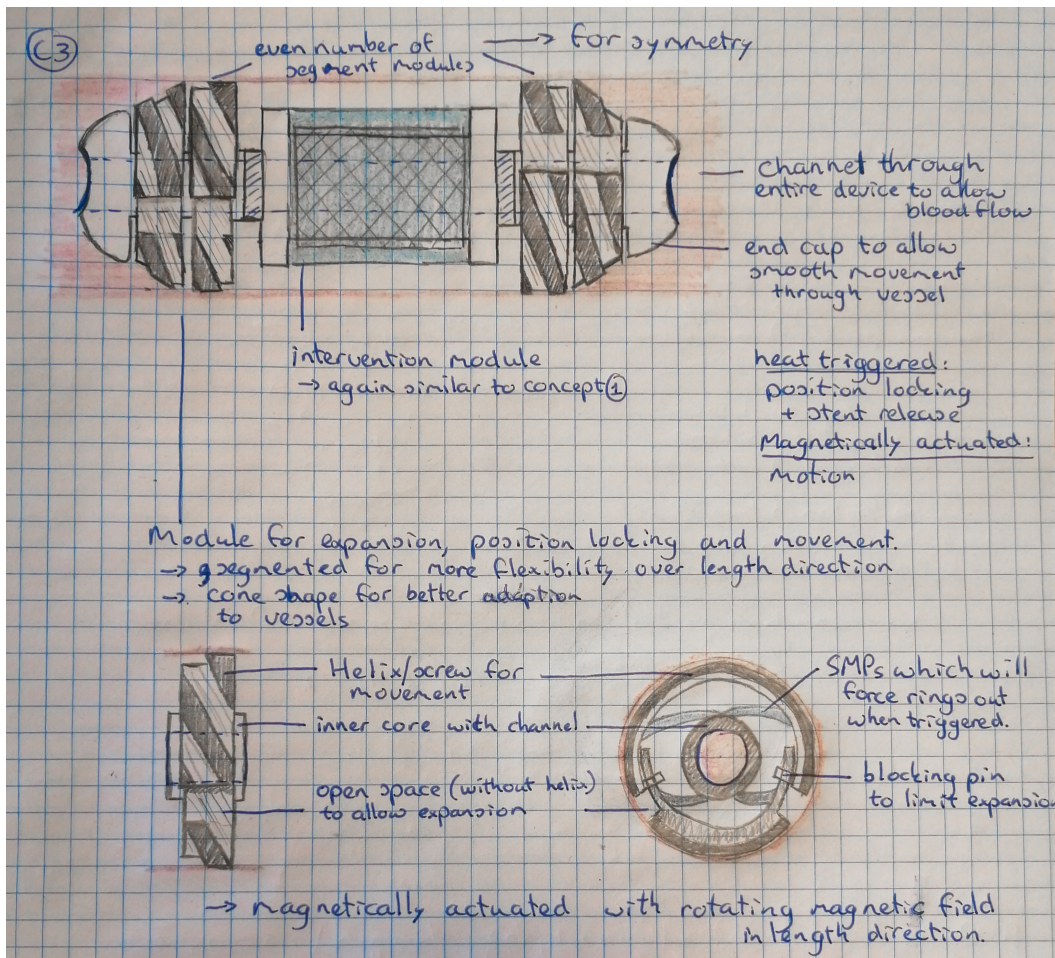


Figure A.9: Hand sketch of full system concept 3 with C-shaped rings and flexible parts for radial adaptation, Shape Memory Polymers (SMPs) for position locking, screw-like threads for movement, and biodegradable capsule for stent placement. See text on image for more explanation.

## C Robosoft Conference Paper

# A Magnetically-Actuated Flexible Capsule Robot for Untethered Cardiovascular Interventions

Gijsbert Michiel van Vliet, Sarthak Misra, Venkatasubramanian Kalpathy Venkiteswaran

**Abstract**—Robotic medical systems have been developed over the last few decades to reduce invasiveness and increase possibilities of minimally invasive surgery (MIS). This paper investigates a new, wireless, magnetically-actuated capsule robot as an untethered tool for cardiovascular surgery. The compliant magnetic capsule robot (CMCR) is designed to navigate larger blood vessels such as the abdominal aorta. Circular flexures provide the CMCR with radial adaptability, and the radial stiffness is analyzed using beam theory to calculate the actuation torque. Axial flexibility is also endowed onto the CMCR using a segmented structure and soft material core. Magnets are embedded on the CMCR to allow wireless actuation. Experiments are performed on prototypes of the CMCR to demonstrate its function as a proof-of-concept. Controlled actuation and adaptability of the CMCR are demonstrated in straight and curved tubes of varying diameters. Actuation of the CMCR in fluid flow and an approach for MIS insertion are also demonstrated to validate its potential for clinical application.

## I. INTRODUCTION

Minimally invasive surgery (MIS) has emerged as an indispensable approach in many surgical disciplines [1], and the advent of robotic surgical devices has expanded the scope and impact of MIS [2], [3]. Recently, the development of robotic devices for surgery has evolved from large rigid platforms towards small, task-specific flexible robots. This improves accessibility to delicate and confined areas in the body which were previously difficult or impossible to reach [4].

Within surgical robotic devices, tethered continuum robots show some favorable MIS characteristics, such as their compliance and the ability to navigate narrow passages [5]–[7]. These properties are utilized in MIS tools like tendon-driven concentric tube robots [8] and magnetic sub-millimeter-diameter guidewires [9]. Nevertheless, tethered devices are limited in maneuverability and are not able to reach and perform surgical tasks in many areas within the body with restricted access [10].

As an alternative to tethered systems, mobile untethered capsule devices have been investigated to reach remote sites in the human body in even less invasive ways. Commercialized wireless capsule endoscopes (e.g., Pillcam®, Medtronic, USA and MiroCam®, IntroMedic Co.,Ltd., South

All authors are affiliated with Surgical Robotics Laboratory, Department of Biomechanical Engineering, University of Twente, 7500 AE Enschede, The Netherlands. Contact: v.kalpathyvenkiteswaran@utwente.nl

S. Misra is also affiliated with the Department of Biomedical Engineering, University of Groningen and University Medical Centre Groningen, 9713 GZ Groningen, The Netherlands.

This research has received funding from the Faculty of Engineering Technology at the University of Twente under the project ‘Symbiobot’.

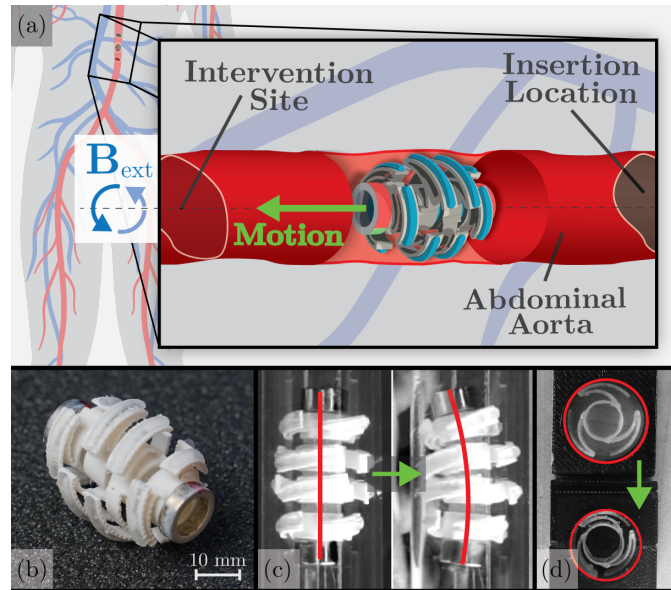


Fig. 1: Overview of the Compliant Magnetic Capsule Robot (CMCR). (a) Conceptual sketch of CMCR moving between the insertion and intervention sites in the abdominal aorta under the influence of a rotational external magnetic field ( $B_{ext}$ ). (b) Prototype of the CMCR. (c) The CMCR has axial flexibility which allows it to bend along its long axis and move through curved vessels. (d) Radial compressibility of the CMCR ensures it maintains contact with the vessel wall when moving through sections of varying diameter.

Korea) have already been accepted in clinics for diagnosis of gastrointestinal diseases [11]–[13]. The clinical functionality of these capsule endoscopes has recently been expanded through the introduction of magnetically-actuated capsule endoscopes (MACEs) which allow active control of the capsule, although they are as yet are unable to perform surgical interventions [14], [15] (NaviCam®, AnX Robotica Corp., USA).

Magnetic actuation has benefits including human-safe operation, wireless actuation and rapid response, and has been investigated for medical applications such as magnetic catheter ablation and electromagnetic navigation bronchoscopy [16], [17]. Untethered soft robots controlled using magnetic fields have demonstrated motion in fluids, manipulate objects in the workspace, and the ability to carry cargo [18]–[20]. Magnetic capsule robots capable of fine-needle biopsy have been developed by combining the benefits of magnetic actuation and soft materials, demonstrating potential for real clinical application [21].

Existing capsule endoscopes focus primarily on the digestive tract [22], [23], including MACEs which allow

active control of the orientation of the capsule using an external magnetic field. Previous research in rigid magnetic capsule robots has considered the use of screw-like motion for controlled motion in air and liquids [24], [25]. However, existing capsule robots lack the ability to navigate vasculature and simultaneously maintain their position within blood vessels to perform surgical tasks in the face of blood flow. It would be beneficial to have robotic capsules that can passively anchor to the blood vessel at a target location, withstanding blood flow while having capabilities to perform surgical interventions.

This paper investigates the design of an untethered capsule robot for interventions in the cardiovascular system (Fig. 1). The compliant magnetically-actuated capsule robot (CMCR) has radial adaptability and stiffness (through curved flexures) to maintain contact with the vessel wall and remain stationary in the face of blood flow. It can be moved along blood vessels of varying diameters using rotating magnetic fields, utilizing a screw-like motion. A segmented structure with a soft material core endows the CMCR with axial flexibility for traversing curved paths. The flexibility of the CMCR can be tuned based on actuation requirements, and it can be inserted in its compressed state for minimally invasive entry during operation. The feasibility of the CMCR is demonstrated as a proof-of-concept for capsule robots towards cardiovascular interventions.

## II. COMPLIANT MAGNETIC CAPSULE DESIGN

In this section, the design of the CMCR is explained in detail. Three attributes — passive radial adaptability, axial flexibility, and active magnetic actuation for movement — are explained. This is followed by an explanation of the fabrication process. An overview of the design and its dimensions can be found in Fig. 2 and Table I.

### A. Radial Adaptability

The capsule robot requires a radially adaptable structure to adjust to the fluctuating diameter of blood vessels. This adaptability is achieved through flexures. Two circular flexures are connected in series to form a flexure pair that provides compliance in the radial direction. One end of the inner flexure is connected to the core, while the outer flexure presses against the vessel wall. The flexure-pairs allow the CMCR to decrease its diameter in small blood vessels under the compressive force from the vessel wall, and expand in larger vessels due to the elasticity of the flexures.

### B. Axial Flexibility

Flexibility in the axial direction of the CMCR is necessary for moving through curved blood vessels. Segmentation of the capsule structure and use of a soft material core allow axial bending of the CMCR. Each segment of the capsule structure consists of circular flexure pairs arranged in groups of three. The soft material core connects these segments while allowing relative bending between them.

### C. Magnetically-Actuated Movement

The CMCR should move steadily through the blood vessel using magnetic actuation. Rotation-based screw-like motion under the influence of a rotating magnetic field is utilized for this motion. To this end, two radially-magnetized permanent magnets are embedded in the CMCR. These magnets create an internal magnetic dipole ( $\mu_{int}$ ) along a radial direction which aligns with an external magnetic field ( $\mathbf{B}_{ext}$ ) (Fig. 2c). Therefore, rotation of the CMCR is induced when the external field is rotated around the longitudinal axis of the CMCR. This rotational motion is transferred to longitudinal motion through the outer circular flexures which form a helical thread with a  $10^\circ$  pitch angle.

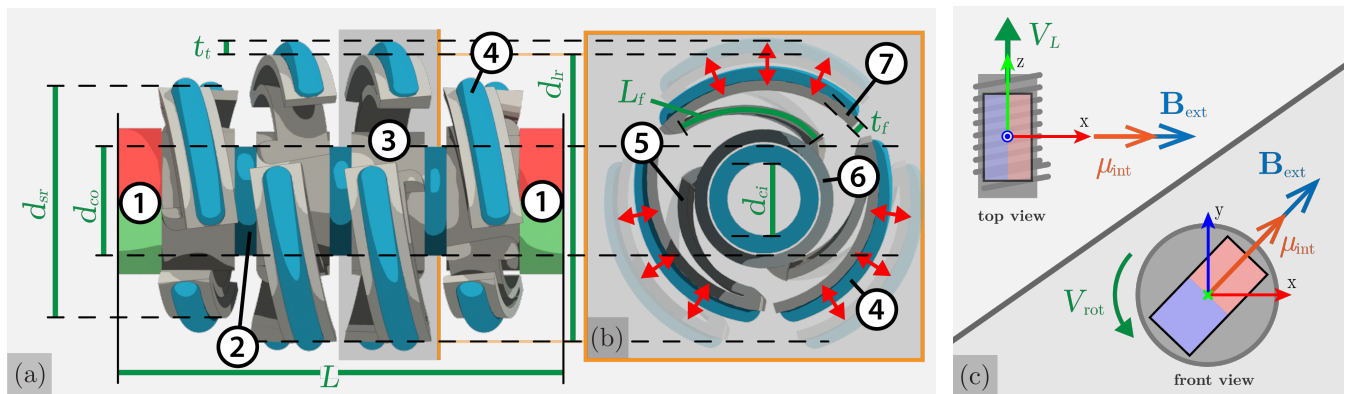


Fig. 2: Design of the compliant magnetic capsule robot (CMCR). (a) Side view of the CMCR and its dimensions: Total capsule length ( $L$ ), flexible thread thickness ( $t_t$ ), flexure thickness ( $t_f$ ), flexure length ( $L_f$ ), large ring OD ( $d_{lr}$ ), small ring OD ( $d_{sr}$ ), flexible core OD ( $d_{co}$ ), and flexible core ID ( $d_{ci}$ ). The capsule design contains: ① permanent magnets, ② a flexible core, and ③ segments of flexure pairs. (b) Front view of the CMCR showing compression of the flexure pairs and passive elastic restoration to the default diameter. The flexure pairs consist of an inner flexure ⑤ and an outer flexure ⑦ in series. A flexible thread ④ is attached to the outer flexure to ensure soft contact with the vessel wall. The inner part of the segment is a rigid core ⑥. (c) Working principle for the CMCR: The internal magnetic dipole of the robot ( $\mu_{int}$ ) aligns with the external magnetic field ( $\mathbf{B}_{ext}$ ). Forward (or backward) motion ( $V_L$ ) is caused by screw-like rotational motion ( $V_{rot}$ ) due to the rotation of the external field.

TABLE I: Dimensions of the three different scaled prototypes of the compliant magnetically-actuated capsule robot (CMCR).

| Dimension                      | Symbol     | Prototype scale |      |      |
|--------------------------------|------------|-----------------|------|------|
|                                |            | 1.00            | 1.25 | 1.50 |
| Uncompressed OD (mm)           |            |                 |      |      |
| - Large ring                   | $d_{lr,u}$ | 20.0            | 24.8 | 30.4 |
| - Small ring                   | $d_{sr,u}$ | 16.0            | 19.8 | 24.3 |
| Compressed OD (mm)             |            |                 |      |      |
| - Large ring                   | $d_{lr,c}$ | 15.0            | 18.6 | 22.8 |
| - Small ring                   | $d_{sr,c}$ | 12.0            | 14.9 | 18.3 |
| Flexure length (mm)            |            |                 |      |      |
| - Large ring                   | $L_{f,lr}$ | 10.0            | 12.5 | 15.0 |
| - Small ring                   | $L_{f,sr}$ | 5.5             | 6.9  | 8.3  |
| Flexure thickness (mm)         | $t_f$      | 0.7             | 0.7  | 0.7  |
| Flexible core OD (mm)          | $d_{co}$   | 7.5             | 9.3  | 11.4 |
| Flexible core ID (mm)          | $d_{ci}$   | 5.0             | 6.2  | 7.6  |
| Flexible thread thickness (mm) | $t_t$      | 1.0             | 1.2  | 1.5  |
| Total capsule length (mm)      | $L$        | 30.5            | 37.7 | 49.2 |

#### D. Prototype Fabrication and Scaling

Prototypes of the CMCR are fabricated using a combination of rapid prototyping techniques. The segments with the flexure-pairs are 3D printed with ABSplus P430 material on the Fortus 250mc FDM printer (Stratsys, Ltd., Eden Prairie, MN, USA). All circular flexures have an arc angle of  $90^\circ$  and a thickness ( $t_f$ ) of 0.7 mm, which was the lowest possible thickness using the 3D printer. The core is 3D printed with Elastic 50A Resin on a Form 2 stereolithography (SLA) printer (Formlabs, Somerville, MA, USA). Elastic 50A Resin is used for these threads to improve the robot's compliance to the tissue of the aortic wall. The threads have a thickness ( $t_t$ ) of 1 mm and are glued to the flexure-pairs.

Three different scaled prototypes of the CMCR design are fabricated to test the performance with respect to stiffness of the circular flexures. A base prototype (1.00 $\times$ ) is created with an uncompressed outer diameter of 20 mm which would be suitable for the abdominal aorta. For the other prototypes, the thickness of the flexures ( $t_f$ ) is kept constant and the other dimensions are scaled to 1.25 $\times$  and 1.50 $\times$  of the base design. The dimensions of all the prototypes can be found in Table I. In the base design, two 10/7 $\times$ 3 mm radially-magnetized ring magnets (Model R-10-07-03-DN, Supermagnete, Gottmadingen, Germany) are embedded in the CMCR. Two 12 $\times$ 6 mm disc magnets with a radial N42 magnetisation (Model S-12-06-DN, Supermagnete, Gottmadingen, Germany) are used for the 1.25 $\times$  and 1.50 $\times$  scale prototypes.

### III. MODELING FLEXURE STIFFNESS

The radial stiffness of the CMCR determines its adaptability to changing vessel diameters and the actuation field necessary to generate motion. In this section, a mathematical model is derived to calculate the stiffness of the flexure pairs on the CMCR.

A single flexure-pair of the capsule robot is modeled as two circular cantilever beams connected in series (Fig. 3a). The outer beam is in contact with the vessel wall, and therefore it is assumed that a distributed force ( $\bar{F}$ ) acts per unit length on the outer beam. The inner beam is fixed at the

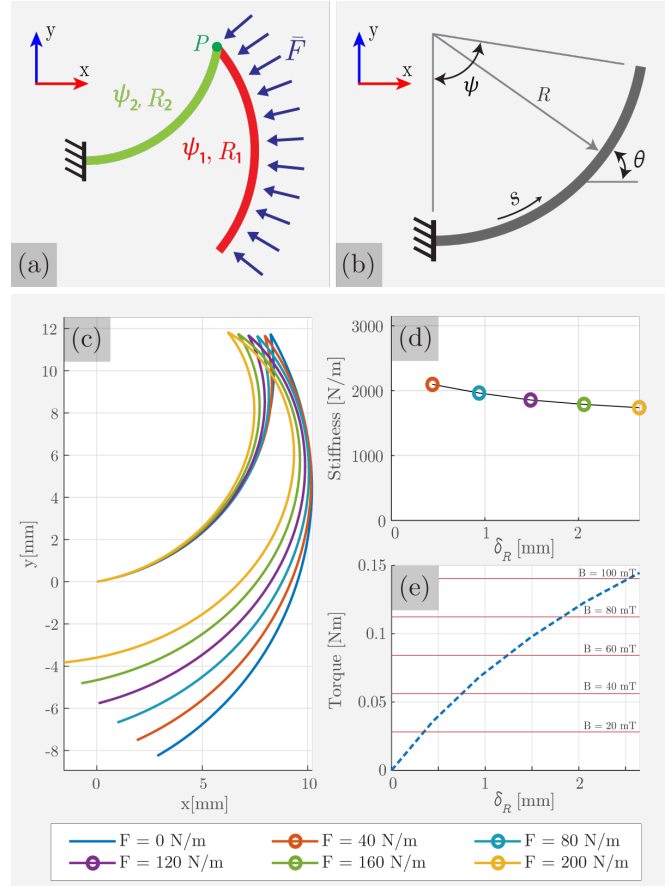


Fig. 3: Stiffness modeling of flexure pairs. (a) The outer flexure experiences a distributed force per unit length ( $\bar{F}$ ), has undeflected radius ( $R_1$ ) and subtends an arc angle ( $\psi_1$ ). The inner flexure is fixed at the root, has undeflected radius ( $R_2$ ) and subtends an arc angle ( $\psi_2$ ). (b) The deflection of each flexure is calculated using beam theory, with  $s$  representing the independent coordinate along the beam length, and  $\theta(s)$  the deflected orientation of the beam at  $s$ . (c) Shapes of the 1.50 $\times$  scale flexure pairs under increasing load. (d) Stiffness of the flexure pair under increasing radial deformation ( $\delta_R$ ). (e) Comparison of stall torque due to friction under increasing radial deformation and maximum torque produced by a magnetic field.

root and the reaction loads from the outer beam act at the tip of the inner beam. For simplicity, only planar deflections (in the  $xy$ -plane as indicated in Fig. 3a) are considered.

For a single beam, the deflection can be characterized using beam theory assuming bending-dominant behavior. Each beam is defined by its radius  $R$  and arc angle  $\psi$ , with arc length  $L = \psi R$ . The independent centerline coordinate  $s \in [0, L]$  and the coordinate-dependent slope  $\theta(s)$  are used to calculate the deflected shape using beam theory as

$$\theta'(s) = \frac{M(s)}{EI} + \frac{1}{R}, \quad (1)$$

with bending moment  $M(s)$ , second moment of area  $I$  and elastic modulus  $E$ . For a rectangular cross-section,  $I = wt^3/12$  with width  $w$  and thickness  $t$ .

For the analysis here, each beam is considered independently, with the deflection and reaction loads on the outer beam calculated first, followed by the inner beam.

Following the methodology described by Venkiteswaran and Su [26], Eqn. (1) is differentiated with respect to the variable  $s$  and combined with two boundary conditions to obtain a set of equations that define beam behavior.

For the outer beam, the derivative of the bending moment in the z-direction is calculated as

$$dM_1^z(s) = \|\mathbf{s}^* \times d\mathbf{F}\|, \quad (2)$$

where

$$d\mathbf{F} = \bar{F} \cdot \begin{bmatrix} -\sin(\theta_1(s)) \\ \cos(\theta_1(s)) \end{bmatrix}, \quad (3)$$

and

$$\mathbf{s}^* = \begin{bmatrix} \int_s^L \cos \theta_1(s) ds \\ \int_s^L \sin \theta_1(s) ds \end{bmatrix}. \quad (4)$$

For planar deflections in the xy-plane, only the z-component of the bending moment acts on the beam. Therefore,

$$\theta_1''(s) = \frac{-dM_1^z(s)}{EI}. \quad (5)$$

For the outer beam, the slope at the fixed end ( $s = 0$ ) is zero. At the end of the beam ( $s = L$ ), the moment  $M_1^z(L_1)$  is zero. Therefore, the boundary conditions are

$$\theta_1(0) = 0, \quad \theta_1'(L_1) = \frac{1}{R_1}. \quad (6)$$

For the inner beam, the reaction force  $\mathbf{F}_P$  and reaction moment  $M_P^z$  at the connection point  $P$  (Fig. 3a) between the two beams must be calculated first. This force and moment are defined as

$$\mathbf{F}_P = \int_0^{L_1} d\mathbf{F} ds = \bar{F} \cdot \int_0^{L_1} \begin{bmatrix} -\sin(\theta_1(s)) \\ \cos(\theta_1(s)) \end{bmatrix} ds, \quad (7)$$

and

$$M_P^z = M_1^z(0). \quad (8)$$

Thus, for the inner beam,

$$\theta_2''(s) = \frac{-dM_2^z(s)}{EI} = \frac{1}{EI} (F_P^x \sin \theta_2(s) - F_P^y \cos \theta_2(s)). \quad (9)$$

The slope at the fixed end of the beam ( $s = 0$ ) is zero. The moment  $M_P$  acts at the other end of the beam ( $s = L$ ). This results in the boundary conditions

$$\theta_2(0) = 0, \quad \theta_2'(L_2) = \frac{M_P^z}{EI} + \frac{1}{R_2}. \quad (10)$$

Eqns. (5),(6),(9) and (10) form a set of differential equations and boundary conditions can be solved using numerical methods. The shape of the deflected beams can be calculated from the  $x$  and  $y$  coordinates as

$$x(s) = \int_s^L \cos \theta(s) ds \quad (11)$$

$$y(s) = \int_s^L \sin \theta(s) ds. \quad (12)$$

With these deflected beam shapes the mean change in radius ( $\delta_R$ ) of the flexure-pair is calculated across 10 points along the length of the outer beam. For a given input force

TABLE II: Parameters for stiffness and actuation analysis for the  $1.50\times$  scale prototype.

| Parameter                   | Value | Parameter                                | Value |
|-----------------------------|-------|--|-------|
| Elastic modulus $E$ (GPa)   | 2.20  | Friction coefficient $\mu_f$             | 0.80  |
| Flexure width $w$ (mm)      | 5.30  | Flexure thickness $t$ (mm)               | 0.70  |
| Flexure 1 radius $R_1$ (mm) | 14.7  | Flexure 2 radius $R_2$ (mm)              | 10.2  |
| Flexure Angle $\psi$ (deg)  | 90.0  | Magnet dipole $\mu_B$ (Am <sup>2</sup> ) | 1.46  |

$F = L_1 \bar{F}$ , the stiffness of the flexure-pair  $k_{fp}$  is defined as

$$k_{fp} = F/\delta_R. \quad (13)$$

The reaction force from compression of the flexure pairs leads to friction between the CMCR and vessel wall. If  $N$  flexure pairs under radial compression  $\delta_R$  are in contact with the vessel wall, the stall torque is given by

$$T_f = \mu_f N k_{fp} \delta_R (R - \delta_R), \quad (14)$$

where  $\mu_f$  is the coefficient of static friction between the CMCR and vessel wall. The CMCR is able to overcome the friction stall torque and move under an external magnetic field  $\mathbf{B}_{\text{ext}}$  if

$$T_f < T_B = \|\mu_{\text{int}} \times \mathbf{B}_{\text{ext}}\|, \quad (15)$$

where  $\mu_{\text{int}}$  is the total magnetic dipole moment of the CMCR and  $T_B$  is the induced magnetic torque.

The above condition can be used to determine the magnetic field necessary to move the CMCR. As an example, this is evaluated for one of the prototypes ( $1.50\times$  scale) and tested under a uniform magnetic field (Sec. IV). The parameters for the analysis are given in Table II. The coefficient of friction is assumed to be 0.8 for contact between the flexible thread made of rubber and the acrylic wall of the tubes used for experiments. The deflection of the flexure-pair is obtained for a range of  $\bar{F} \in [0, 200]$  N/m (Fig. 3c). It is noticeable that most of the deformation is concentrated on the outer flexure. The stiffness of the flexure-pairs decreases under deformation, as can be seen in Fig. 3d. The comparison between maximum magnetic torque and friction stall torque is given in Fig. 3e. For the  $1.50\times$  scale prototype, a magnetic field of 100 mT can move the CMCR under 2.5 mm radial compression.

#### IV. EXPERIMENTS AND RESULTS

Experiments are performed on the prototypes to demonstrate the motion of the CMCR under a rotating magnetic field, and also its radial adaptability, axial flexibility and potential for application in minimally invasive surgery. **(Please refer to the Supplementary Video).**

##### A. Motion experiments

The motion of the CMCR is tested in tubes of different shapes. The magnetic field in these experiments is generated with a  $\emptyset 60$  mm N42 disc magnet (Model S-60-05-DN, Supermagnete, Gottmadingen, Germany). Tubes of different inner diameter (ID) are used to demonstrate motion in various states of radial compression of the CMCR, and all three scaled prototypes are tested.

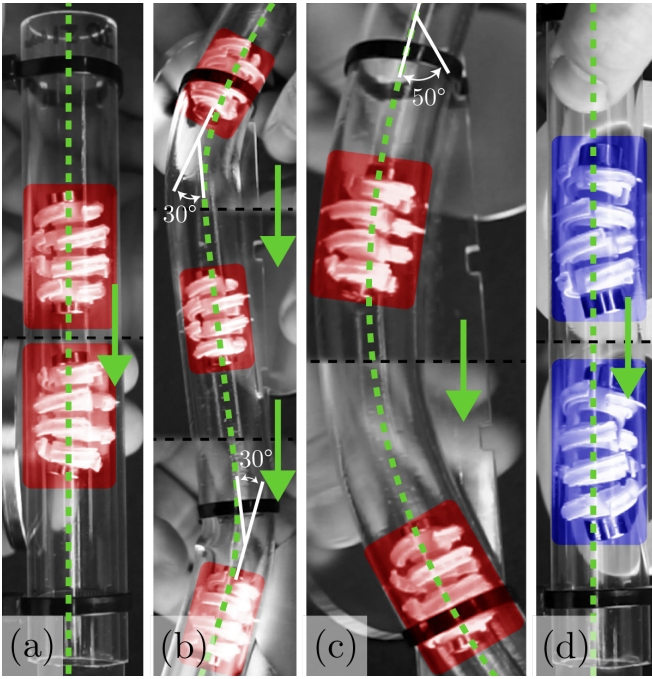


Fig. 4: Motion experiments with a handheld disc magnet:  $1.00\times$  scale prototype (uncompressed) in a tube of inner diameter 21 mm for (a) straight-line motion, (b) motion through S-shape with  $30^\circ$  bends, and (c) motion through  $50^\circ$  curve. (d)  $1.25\times$  scale prototype (compressed) in tube of 21 mm inner diameter demonstrating straight-line motion.

Figure 4 shows results from these experiments. The CMCR moves due to the rotation induced by the external magnetic field in compressed and uncompressed states. The different prototypes are initially tested in straight tubes, followed by a tube with an S-shape with two sharp  $30^\circ$  bends and another tube has a gradual  $50^\circ$  circular curve. In all experiments, the CMCR is able to move forward and backward by reversing the direction of rotation of the magnet. However, slippage is occasionally observed due to attractive forces from the disc magnet.

In addition, some experiments are executed in a setup with electromagnets (BigMag [27]) to test the performance of the capsule robot in controlled magnetic fields up to 50 mT. The motion of different scaled prototypes of CMCR is tested in straight tubes at different states of compression. It is observed that the  $1.50\times$  prototype moves under the generated magnetic field (up to 50 mT) in partially compressed states, tallying with the theoretical analysis in Sec. III (**Please refer to Supplementary Video**). The  $1.25\times$  prototype also demonstrates motion in some compressed states under this magnetic field. However, the  $1.00\times$  prototype can only move under this field when uncompressed.

### B. Additional Experiments

The ability of the CMCR to move through sections of varying diameter is tested using a tapered tube made from silicone (Fig. 5a). The inner diameter of the tube changes from 26 mm to 21 mm over a length of 100 mm. The  $1.25\times$  scale prototype is moved forward and back through the tube, but the motion is restricted partway along the length.

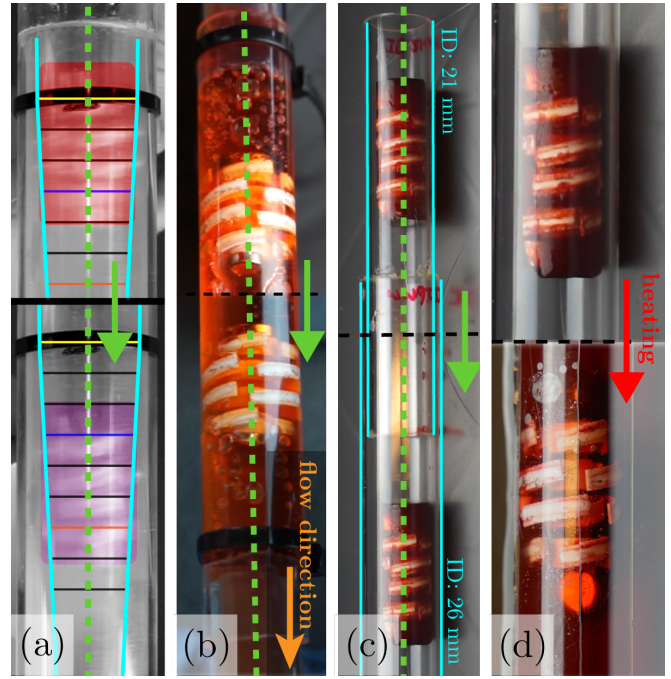


Fig. 5: (a) Motion of compliant magnetic capsule robot (CMCR) in a tapered tube from an uncompressed state (red box) up to a partly compressed state (purple box). (b) Motion test in the fluid flow. (c) Insertion of the compressed CMCR encapsulated in ice from inner diameter (ID) 21 mm tube to ID26 mm tube. (d) Releasing CMCR from ice using water to expand to 26 mm.

Since the intended application is cardiovascular interventions, the motion of the CMCR in flowing liquid is also tested. Water with red dye is used as the liquid, and the setup is connected to a pump that cycles the water at 2.9 L/min, flow rate of blood through the abdominal aorta. The  $1.00\times$  scale prototype is tested in a tube with inner diameter 21 mm in the uncompressed state (Fig. 5b). The CMCR holds steady in the flowing water, and only moves when the rotating magnetic field is applied. Additionally, it does not block the flow of liquid.

In order to demonstrate an approach for minimally invasive insertion of the CMCR, the  $1.25\times$  scale prototype is fully compressed and embedded in a block of ice with an outer diameter of 20 mm. It is then inserted through a tube of inner diameter 21 mm and guided to a larger tube with a diameter of 26 mm using a magnet (Fig. 5c). Once at the target location, the ice capsule is melted with water, which releases the flexures and causes the CMCR to anchor in place within the larger tube (Fig. 5d).

## V. DISCUSSION

The experimental results show that the CMCR is able to move through both straight and curved tubes in both compressed and uncompressed states. However, the motion is more difficult when the diameter of the tube decreases due to increased friction. This is observed in the experiments in BigMag where the stiffer  $1.00\times$  prototype can only produce limited motion under a uniform 50 mT field. The handheld magnets can produce fields up to 100 mT, which is demonstrated to be sufficient to move all three prototypes.

Friction with the vessel wall is one of the primary design considerations for the CMCR. With decreasing vessel diameter, the flexures are compressed more, which causes increase in reaction forces with the wall and consequently friction. The friction is beneficial in ensuring the capsule stays in place under fluid flow or other disturbances. However, increase in friction also leads to increase in actuation magnetic torque needed to generate rotational motion. The dimensions and material of the flexures determine the compression stiffness of the CMCR and therefore the friction force. In this study, the design was limited by fabrication constraints imposed by 3D printing, but it can be improved with a customized fabrication protocol. Increasing the size or volume of the permanent magnets on the CMCR will also help increase actuation torque.

Slippage of the CMCR is observed occasionally in both compressed and uncompressed tests. This undesirable slippage occurs due to attractive forces from the external permanent magnet. This issue can be overcome using an actuation system which can generate a more uniform magnetic field. Excessive axial bending of the CMCR (from the soft material core) is also observed during actuation, which limits the efficiency of motion. While axial flexibility is necessary for navigating bends, it must be optimized for ideal performance. This can be achieved by altering the dimensions or material of the flexible core.

## VI. CONCLUSIONS & FUTURE WORK

In this paper, a combination of flexures, soft materials and magnets are used to design a capsule robot (CMCR) with a flexible structure that can be controlled wirelessly. The CMCR moves through curved and straight tubular structures using screw-like motion under actuation from a rotating magnetic field. The actuation field can be calculated using the stiffness of the flexures. The CMCR can also move through tubes with varying diameters and in an environment with flowing liquid. The  $1.00\times$  scale prototype presented here is suitable for the abdominal aorta, with an uncompressed outer diameter of 20 mm. The maximum possible diameter change of the CMCR for all three scaled prototypes is 25%. which may be improved with a smaller core.

The experiments with fluid flow and minimally invasive insertion of the CMCR suggest potential for clinical application. However, this requires further optimization of the design in terms of materials and dimensions. Improved fabrication techniques can help produce parts at smaller scales and with better resolution. The compliance of the flexures must be tuned for suitability in real blood vessels. For use in robotic surgery, the CMCR must also be embedded with sensors and surgical tools. The CMCR can provide a template for wireless robots that can serve surgical applications such as diagnostic imaging and artherectomy.

## REFERENCES

- [1] J. Wickham, "Minimally Invasive Surgery," *Journal of Endourlogy*, vol. 1, no. 2, pp. 71–74, 1987.
- [2] R. Beasley, "Medical Robots: Current Systems and Research Directions," *Journal of Robotics*, vol. 2012, pp. 1–14, 2012.
- [3] Vitiello *et al.*, "Emerging robotic platforms for minimally invasive surgery," *IEEE Reviews in Biomedical Engineering*, vol. 6, pp. 111–126, 2013.
- [4] Sitti *et al.*, "Biomedical Applications of Untethered Mobile Milli/Microrobots," *Proceedings of the IEEE*, vol. 103, no. 2, pp. 205–224, 2015.
- [5] Burgner-Kahrs *et al.*, "Continuum Robots for Medical Applications: A Survey," *IEEE Transactions on Robotics*, vol. 31, no. 6, pp. 1261–1280, Dec. 2015.
- [6] Thomas *et al.*, "Surgical Applications of Compliant Mechanisms: A Review," *Journal of Mechanisms and Robotics*, vol. 13, no. 2, p. 020801, 2021.
- [7] Runciman *et al.*, "Soft Robotics in Minimally Invasive Surgery," *Soft Robotics*, vol. 6, no. 4, pp. 423–443, 2019.
- [8] Bedell *et al.*, "Design optimization of concentric tube robots based on task and anatomical constraints," *Proceedings - IEEE International Conference on Robotics and Automation*, pp. 398–403, 2011.
- [9] Jeon *et al.*, "A Magnetically Controlled Soft Microrobot Steering a Guidewire in a Three-Dimensional Phantom Vascular Network," *Soft Robotics*, vol. 6, no. 1, pp. 54–68, 2019.
- [10] Nelson *et al.*, "Microrobots for Minimally Invasive Medicine," *Annual Review of Biomedical Engineering*, vol. 12, no. 1, pp. 55–85, 2010.
- [11] Iddan *et al.*, "Wireless capsule endoscopy," *Nature*, vol. 405, no. 6785, pp. 417–418, May 2000.
- [12] Singeap *et al.*, "Capsule endoscopy: The road ahead," *World Journal of Gastroenterology*, vol. 22, no. 1, pp. 369–378, Jan. 2016.
- [13] Ciuti *et al.*, "Frontiers of robotic endoscopic capsules: a review," *Journal of Micro-Bio Robotics*, vol. 11, no. 1–4, pp. 1–18, Jun. 2016.
- [14] A. Mahoney and J. J. Abbott, "Five-degree-of-freedom manipulation of an untethered magnetic device in fluid using a single permanent magnet with application in stomach capsule endoscopy," *The International Journal of Robotics Research*, vol. 35, no. 1–3, pp. 129–147, 2016.
- [15] Zhao *et al.*, "Screening for gastric cancer with magnetically controlled capsule gastroscopy in asymptomatic individuals," *Gastrointestinal Endoscopy*, vol. 88, no. 3, pp. 466–474, Sep. 2018.
- [16] Ernst *et al.*, "Initial experience with remote catheter ablation using a novel magnetic navigation system: magnetic remote catheter ablation," *Circulation*, vol. 109, no. 12, pp. 1472–1475, 2004.
- [17] Gildea *et al.*, "Electromagnetic navigation diagnostic bronchoscopy: a prospective study," *American Journal of Respiratory and Critical Care Medicine*, vol. 174, no. 9, pp. 982–989, 2006.
- [18] Hu *et al.*, "Small-scale soft-bodied robot with multimodal locomotion," *Nature*, vol. 554, no. 7690, pp. 81–85, 2018.
- [19] Venkiteswaran *et al.*, "Tandem actuation of legged locomotion and grasping manipulation in soft robots using magnetic fields," *Extreme Mechanics Letters*, vol. 41, p. 101023, 2020.
- [20] Lu *et al.*, "A bioinspired multilegged soft millirobot that functions in both dry and wet conditions," *Nature Communications*, vol. 9, no. 1, p. 3944, 2018.
- [21] Son *et al.*, "Magnetically Actuated Soft Capsule Endoscope for Fine-Needle Biopsy," *Soft Robotics*, vol. 7, no. 1, pp. 10–21, 2020.
- [22] Yim *et al.*, "Biopsy using a magnetic capsule endoscope carrying, releasing, and retrieving untethered microgrippers," *IEEE Transactions on Biomedical Engineering*, vol. 61, no. 2, pp. 513–521, 2014.
- [23] Pham *et al.*, "Soft Endoluminal Robots Propelled by Rotating Magnetic Dipole Fields," *IEEE Transactions on Medical Robotics and Bionics*, vol. 2, no. 4, pp. 598–607, 2020.
- [24] Popek *et al.*, "Six-Degree-of-Freedom Localization of an Untethered Magnetic Capsule Using a Single Rotating Magnetic Dipole," *IEEE Robotics and Automation Letters*, vol. 2, no. 1, pp. 305–312, 2017.
- [25] Nam *et al.*, "Magnetic helical robot for targeted drug-delivery in tubular environments," *IEEE/ASME Transactions on Mechatronics*, vol. 22, no. 6, pp. 2461–2468, Dec. 2017.
- [26] V. Venkiteswaran and H. J. Su, "Pseudo-rigid-body models for circular beams under combined tip loads," *Mechanism and Machine Theory*, vol. 106, pp. 80–93, 2016.
- [27] Sikorski *et al.*, "Introducing BigMag - A novel system for 3D magnetic actuation of flexible surgical manipulators," *Proceedings - IEEE International Conference on Robotics and Automation*, pp. 3594–3599, Jul. 2017.